

# Why there are no elliptical galaxies more flattened than $E7$ . Thirty years later

R. Caimmi\*

November 12, 2018

## Abstract

Elliptical galaxies are modelled as homeoidally striated Jacobi ellipsoids (Caimmi & Marmo 2005) where the peculiar velocity distribution is anisotropic, or equivalently as their adjoints configurations i.e. classical Jacobi ellipsoids of equal mass and axes, in real or imaginary rotation (Caimmi 2006). Reasons for the coincidence of bifurcation points from axisymmetric to triaxial configurations in both the sequences (Caimmi 2006), contrary to earlier findings (Wiegandt 1982a,b; Caimmi & Marmo 2005) are presented and discussed. The effect of centrifugal support at the ends of the major equatorial axis, is briefly outlined. The existence of a lower limit to the flattening of elliptical galaxies is investigated in dealing with a number of limiting situations. More specifically, (i) elliptical galaxies are considered as isolated systems, and an allowed region within Ellipsoidland (Hunter & de Zeeuw 1997), related to the occurrence of bifurcation points from ellipsoidal to pear-shaped configurations, is shown to be consistent with observations; (ii) elliptical galaxies are considered as embedded within dark matter haloes and, under reasonable assumptions, it is

---

\*Astronomy Department, Padua Univ., Vicolo Osservatorio 2, I-35122 Padova, Italy  
email: caimmi@pd.astro.it

shown that tidal effects from hosting haloes have little influence on the above mentioned results; (iii) dark matter haloes and embedded elliptical galaxies, idealized as a single homeoidally striated Jacobi ellipsoid, are considered in connection with the cosmological transition from expansion to relaxation, by generalizing an earlier model (Thuan & Gott 1975), and the existence of a lower limit to the flattening of relaxed (oblate-like) configurations, is established. On the other hand, no lower limit is found to the elongation of relaxed (prolate-like) configurations, and the observed lack of elliptical galaxies more elongated than  $E7$  needs a different physical interpretation, such as the occurrence of bending instabilities (Polyachenko & Shukhman 1979; Merritt & Hernquist 1991).

*keywords - cosmology: dark matter - galaxies: evolution - galaxies: formation - galaxies: haloes - galaxies: structure.*

## 1 Introduction

Large-scale celestial objects, represented as self-gravitating fluids, exhibit different features according if their subunits, or “particles”, are conceived as “collisional” or “collisionless”.

In the former alternative, the gravitational field that is generated by the system as a whole is negligible in respect of the force between two colliding subunits, when they repel each other strongly. Consequently, particles in self-gravitating, collisional fluids, are subjected to violent and short-lived accelerations as they are sufficiently close to each other, interspersed with longer periods when they move at nearly constant velocity.

In the latter alternative, the gravitational field that is generated by the system as a whole is dominant in respect of the force between two subunits, even if they are close to each other. Consequently, particles in self-gravitating, collisionless fluids, are subjected to smooth and long-lived accelerations through their trajectories.

Gas in stars and stars in stellar systems may be approximated, to a good extent, as collisional and collisionless, ideal self-gravitating fluids, respectively. The statistical problem of particle motion in the latter case is that of the former, with the collisions left out. “Ideal” has to be intended as “particles collide as perfectly and undeformable spheres” in the former situation, and “particles do not interact each other at all” in the latter.

The motion equation of fluid flow turns out to be the same for both collisional and collisionless fluids (e.g., Jeans 1929, Chap. II, § 26, Chap. VII, §§ 211-215; Binney & Tremaine 1987, Chap. 4, § 4.2) provided gases are thought of as far from equilibrium. Then the velocity distribution of molecules no longer obeys the Maxwell distribution and is, in general, anisotropic; accordingly, the pressure is represented by a stress tensor. In the special case of isotropic velocity distributions, the pressure attains its usual meaning and the motion equation reduces to the Euler's equation, provided the velocity of an infinitesimal fluid element is intended as the mean velocity of all the particles within the same element at the time considered. On the contrary, the Euler's equation for a given fluid with isotropic distribution can be generalized to an anisotropic one, by replacing velocities with mean velocities and pressures with stress tensors, in the sense specified above.

For special classes of ideal, self-gravitating fluids, such as steadily rotating polytropes with polytropic index  $n \geq 1/2$  (Vandervoort 1980a) and isothermal spheres (e.g., Binney & Tremaine 1987, Chap. 4, § 4.4b), a one-to-one correspondence has been discovered between collisional and collisionless systems with equal physical parameters. Steadily rotating polytropes may be represented, to a first extent, as steadily rotating, homeoidally striated ellipsoids (e.g., Vandervoort 1980b; Vandervoort & Welty 1981; Lai et al. 1993).

Though most astronomical bodies exhibit ellipsoidal-like shapes and isopycnic surfaces, still some caution must be used in dealing with the above approximation, with regard to local values of physical parameters. This is why steadily rotating polytropes are in hydrostatic equilibrium while, owing to the Hamy's theorem (e.g., Chambat 1994), the contrary holds for their homeoidally striated ellipsoidal counterparts. On the other hand, homeoidally striated ellipsoids may safely be assumed as a viable approximation to self-gravitating fluids, with regard to typical values of physical parameters, averaged over the whole volume<sup>1</sup> (e.g., Vandervoort 1980b; Vandervoort & Welty 1981; Lai et al. 1993).

Large-scale, celestial objects have been modelled as collisional, self-gravitating fluids, in particular homeoidally striated ellipsoids, since the beginning of their classification (see e.g., Chandrasekhar 1969, Chap. 1). The evidence

---

<sup>1</sup>An important exception is the energy ratio of rotational to random motions,  $E_{\text{rot}}/E_{\text{pec}}$  (Caimmi 1979, 1983).

of rotation in spiral galaxies and the symmetry of figure shown by elliptical galaxies and spiral bulges, suggested the following (e.g., Jeans 1929, Chap. XIII, § 299): (i) all (regular) galaxies rotate; (ii) the symmetry of figure is precisely such as rotation might be expected to produce; (iii) the observed shapes of (regular) galaxies can be explained as the figures assumed by masses rotating under their own gravitation. In particular, the system of primeval stars must have conserved roughly the same shape as the original mass of gas from which it emerged (e.g., Blaauw 1965). The lack of elliptical galaxies more flattened than  $E7$  was explained in a classical paper (Thuan & Gott 1975) where virialized elliptical galaxies and their parent density perturbations are modelled as MacLaurin spheroids and homogeneous, rigidly rotating spheres, respectively.

Since then, observations began to yield increasing evidence that (giant) elliptical galaxies cannot be sustained by systematic rotation (e.g., Bertola & Capaccioli 1975; Binney 1976; Illingworth 1977, 1981; Schechter & Gunn 1979). Accordingly, (giant) elliptical galaxies were conceived as collisionless, self-gravitating fluids, with triaxial<sup>2</sup> boundaries set by specific anisotropic peculiar velocity distribution of stars (Binney 1976, 1978, 1980), and a negligible contribution from figure rotation. Owing to high-resolution simulations, the same holds also for (nonbaryonic) dark matter haloes hosting galaxies and cluster of galaxies (e.g., Hoeft et al. 2004; Rasia et al. 2004; Bailin & Steinmetz 2004).

Isotropic peculiar velocity distributions necessarily imply configurations which rotate around the minor axis. Accordingly, empirical evidence of systematic rotation around the major axis (e.g., Bertola & Galletta 1978), in absence of tidal potential, makes a signature of the occurrence of anisotropic peculiar velocity distribution.

Though anisotropy in peculiar velocity distribution is a basic ingredient in the description and investigation of stellar systems and hosting dark matter haloes, still no attempt (to the knowledge of the author) has been made to explain why elliptical galaxies more flattened than  $E7$  do not exist, following the same line of thought as in Thuan & Gott (1975), with regard to collisionless fluids. This paper aims to address this lack, and is based on a theory

---

<sup>2</sup>Strictly speaking, all tridimensional bodies may be conceived as triaxial, in particular spheres and spheroids. Throughout this paper, “triaxial” shall be intended as denoting ellipsoids where the axes are different in length.

that systematic and random motions are unified (Caimmi 2006, hereafter quoted as C06<sup>3</sup>). To this aim, the procedure used by Thuan & Gott (1975) shall be extended from MacLaurin spheroids to homeoidally striated Jacobi ellipsoids (Caimmi & Marmo 2005, hereafter quoted as CM05<sup>4</sup>), where the effect of peculiar motion excess, implying anisotropic peculiar velocity distribution, is equivalent to the effect of additional (real or imaginary) rotation, related to isotropic peculiar velocity distribution (C06).

An alternative explanation for the absence of elliptical galaxies (and non-baryonic dark matter haloes) more flattened or elongated than  $E7$  as due to bending instabilities, has been suggested long time ago from analytical considerations involving homogeneous (oblate and prolate) spheroids (Polyachenko & Shukhman 1979; Fridman & Polyachenko 1984, Vol. 1, Chap. 4, Sect. 3.3, see also pp. 313-322; Vol. 2, p. 159) and numerical simulations involving inhomogeneous (oblate and prolate) spheroids (Merritt & Hernquist 1991; Merritt & Sellwood 1994).

In a cosmological scenario (Thuan & Gott 1975), the occurrence of a limiting ellipticity in oblate configurations depends on the amount of spin growth regardless from the onset of bending instabilities. An interesting question could be if a similar conclusion holds for prolate configurations. It will be seen that the onset of bending instabilities is necessary for the occurrence of a limiting ellipticity in prolate configurations.

This paper is structured in the following manner. The general theory of homeoidally striated Jacobi ellipsoids, and the relevant results, are outlined in Sect. 2. A unified theory of systematic and random motions, implying a definition of imaginary rotation, and the relevant results, are outlined in Sect. 3. An extension of Thuan & Gott (1975) procedure to homeoidally striated Jacobi ellipsoids in real or imaginary rotation, and the relevant results, are outlined in Sect. 4. The existence of a lower limit to the flattening of elliptical galaxies is investigated in Sect. 5 taking into consideration a number of simplified situations, namely (i) elliptical galaxies as isolated systems; (ii) elliptical galaxies as embedded in dark matter haloes; (iii) dark matter haloes and hosted elliptical galaxies, idealized as a single homeoidally striated Jacobi ellipsoid, in connection with the cosmological transition from

---

<sup>3</sup>A more extended file including an earlier version of the current paper is available at the arxiv electronic site, as astro-ph/0507314.

<sup>4</sup>A more extended version is available at the arxiv electronic site, as astro-ph/0505306.

expansion to relaxation. Some concluding remarks are drawn in Sect. 6, and a few arguments are treated with more detail in the Appendix.

## 2 General theory

### 2.1 Homeoidally striated Jacobi ellipsoids

A general theory for homeoidally striated density profiles has been developed in earlier approaches (Roberts 1962; Caimmi 1993a; Caimmi & Marmo 2003, hereafter quoted as CM03; CM05), and an interested reader is addressed therein for deeper insight. What is relevant for the current investigation, shall be mentioned and further developed here.

The isopycnic (i.e. constant density) surfaces are defined by the following law:

$$\rho = \rho_0 f(\xi) ; \quad f(1) = 1 ; \quad \rho_0 = \rho(1) ; \quad (1a)$$

$$\xi = \frac{r}{r_0} ; \quad 0 \leq \xi \leq \Xi ; \quad \Xi = \frac{R}{r_0} ; \quad (1b)$$

where  $\rho_0$ ,  $r_0$ , are a scaling density and a scaling radius, respectively, related to a reference isopycnic surface,  $\xi$  is a scaled distance, independent of the direction along which radial coordinates are calculated, and  $\Xi = \xi(r)$ , is related to the boundary, where  $r = R$ . Both cored and cuspy density profiles, according to the explicit expression chosen for the scaled density,  $f(\xi)$ , are represented by Eqs. (1). For the cored profiles, a different normalization is used here with respect to Caimmi (1993a), where  $\xi = r/R$  and  $\rho_0$  is the central density.

The mass, the inertia tensor, and the potential self-energy tensor are:

$$M = \nu_{\text{mas}} M_0 ; \quad (2)$$

$$I_{pq} = \delta_{pq} \nu_{\text{inr}} M a_p^2 ; \quad (3)$$

$$(E_{\text{sel}})_{pq} = -\frac{GM^2}{a_1} \nu_{\text{sel}} (B_{\text{sel}})_{pq} = -\frac{GM^2}{a_1} \mathcal{S}_{pq} ; \quad (4)$$

$$E_{\text{sel}} = \sum_{i=1}^3 (E_{\text{sel}})_{ii} = -\frac{GM^2}{a_1} \nu_{\text{sel}} B_{\text{sel}} = -\frac{GM^2}{a_1} \mathcal{S} ; \quad (5)$$

$$(B_{\text{sel}})_{pq} = \delta_{pq} \epsilon_{p2} \epsilon_{p3} A_p ; \quad B_{\text{sel}} = \sum_{s=1}^3 \epsilon_{s2} \epsilon_{s3} A_s ; \quad (6)$$

$$\mathcal{S}_{pq} = \nu_{\text{sel}}(B_{\text{sel}})_{pq} ; \quad \mathcal{S} = \nu_{\text{sel}} B_{\text{sel}} ; \quad (7)$$

where  $\delta_{pq}$  is the Kronecker symbol;  $G$  is the constant of gravitation;  $\nu_{\text{mas}}$ ,  $\nu_{\text{inrr}}$ ,  $\nu_{\text{sel}}$ , are profile factors i.e. depend only on the density profile via the scaled radius,  $\Xi$ ;  $a_1, a_2, a_3$ , are semiaxes;  $\epsilon_{pq} = a_p/a_q$  are axis ratios;  $A_1, A_2, A_3$ , are shape factors i.e. depend only on the axis ratios; and  $M_0$  is the mass of a homogeneous ellipsoid with same density and boundary as the reference isopycnic surface:

$$M_0 = \frac{4\pi}{3} \rho_0 a_{01} a_{02} a_{03} ; \quad (8)$$

where  $a_{01}, a_{02}, a_{03}$ , are the semiaxes of the ellipsoid bounded by the reference isopycnic surface. The combination of Eqs. (1b), (2), and (8) yields:

$$\frac{\bar{\rho}}{\rho_0} = \frac{\nu_{\text{mas}}}{\Xi^3} ; \quad (9)$$

where  $\bar{\rho} = 3M/(4\pi a_1 a_2 a_3)$  is the mean density of the ellipsoid.

The limiting case of homogeneous configurations reads:

$$f(\xi) = 1 , \quad 0 \leq \xi \leq \Xi ; \quad (10a)$$

$$\nu_{\text{mas}} = \Xi^3 ; \quad \nu_{\text{inrr}} = \frac{1}{5} ; \quad \nu_{\text{sel}} = \frac{3}{10} ; \quad (10b)$$

for further details, see CM03, CM05.

## 2.2 Systematic rotation

In dealing with angular momentum and rotational energy, the preservation of (triaxial) ellipsoidal shape imposes severe constraints on the rotational velocity field. In the special case of homeoidally striated Jacobi ellipsoids, the systematic velocity field is defined by the law (CM05):

$$\frac{v_{\text{rot}}(r, \theta, \phi)}{v_{\text{rot}}(R, \theta, \phi)} = \frac{v_{\text{rot}}(a'_1, \pi/2, 0)}{v_{\text{rot}}(a_1, \pi/2, 0)} ; \quad (11)$$

or equivalently, the angular (with respect to  $x_3$  axis) velocity field is defined by the law:

$$\frac{\Omega(r, \theta, \phi)}{\Omega(R, \theta, \phi)} = \frac{\Omega(a'_1, \pi/2, 0)}{\Omega(a_1, \pi/2, 0)} ; \quad (12)$$

where  $(r, \theta, \phi)$ ,  $(R, \theta, \phi)$ , represent a point on a generic isopycnic surface and on the boundary, respectively, along a fixed radial direction, and  $(a'_1, \pi/2, 0)$ ,  $(a_1, \pi/2, 0)$ , represent the end of the major equatorial semiaxis.

It is worth noticing that the following special cases are described by Eqs. (11) or (12): (a) rigid rotation; (b) constant rotation velocity everywhere; (c) rigid rotation of isopycnic surfaces and constant rotation velocity on the equatorial plane. To maintain ellipsoidal shapes, differential rotation [e.g., cases (b) and (c) above] must necessarily be restricted to axysymmetric figures i.e. spheroidal configurations. In the limiting situation of homogeneous, rigidly rotating, dynamical (or hydrostatic) equilibrium configurations, homeoidally striated Jacobi ellipsoids reduce to classical Jacobi ellipsoids (CM05).

The angular-momentum vector and the rotational-energy tensor are:

$$J_s = \delta_{s3}\eta_{anm}\nu_{anm}Ma_p(1 + \epsilon_{qp}^2)(v_{\text{rot}})_p ; \quad p \neq q \neq s ; \quad (13)$$

$$(E_{\text{rot}})_{pq} = \delta_{pq}(1 - \delta_{p3})\eta_{\text{rot}}\nu_{\text{rot}}M[(v_{\text{rot}})_p]^2 ; \quad (14)$$

and the related module and trace, respectively, read:

$$J = \eta_{anm}\nu_{anm}M(1 + \epsilon_{21}^2)a_1(v_{\text{rot}})_1 ; \quad (15)$$

$$E_{\text{rot}} = \eta_{\text{rot}}\nu_{\text{rot}}M(1 + \epsilon_{21}^2)[(v_{\text{rot}})_1]^2 ; \quad (16)$$

where  $\eta_{anm}$ ,  $\eta_{\text{rot}}$ , are shape factors,  $\nu_{anm}$ ,  $\nu_{\text{rot}}$ , are profile factors,  $(v_{\text{rot}})_p$  is the rotational velocity at the end of the semiaxis,  $a_p$ ,  $p = 1, 2$ , and the rotation axis has been chosen to be  $x_3$ . For further details, see CM03, CM05.

The combination of Eqs. (15) and (16) yields:

$$(E_{\text{rot}})_{pq} = \frac{J^2}{Ma_1^2}\nu_{\text{ram}}(B_{\text{ram}})_{pq} = \frac{J^2}{Ma_1^2}\mathcal{R}_{pq} ; \quad (17a)$$

$$\nu_{\text{ram}} = \frac{\nu_{\text{rot}}}{\nu_{anm}^2} ; \quad (17b)$$

$$(B_{\text{ram}})_{pq} = \delta_{pq}(1 - \delta_{p3})\frac{\eta_{\text{rot}}}{\eta_{anm}^2}\frac{\epsilon_{p1}^2}{(1 + \epsilon_{21}^2)^2} ; \quad (17c)$$

$$\mathcal{R}_{pq} = \nu_{\text{ram}}(B_{\text{ram}})_{pq} ; \quad (17d)$$

which makes an alternative expression of the rotation-energy tensor, and:

$$E_{\text{rot}} = \frac{J^2}{Ma_1^2}\nu_{\text{ram}}B_{\text{ram}} = \frac{J^2}{Ma_1^2}\mathcal{R} ; \quad (18a)$$

$$B_{\text{ram}} = \frac{\eta_{\text{rot}}}{\eta_{\text{anm}}^2} \frac{1}{1 + \epsilon_{21}^2} ; \quad (18\text{b})$$

$$\mathcal{R} = \nu_{\text{ram}} B_{\text{ram}} ; \quad (18\text{c})$$

which makes an alternative expression of the rotation energy.

The limiting situations outlined above, read:

$$\nu_{\text{anm}} = \nu_{\text{rot}} = \nu_{\text{inr}} = \frac{1}{5} ; \quad \nu_{\text{ram}} = \nu_{\text{inr}}^{-1} = 5 ; \quad (19)$$

for homogeneous configurations in rigid rotation, according to case (a);

$$\nu_{\text{anm}} = \frac{1}{4} ; \quad \nu_{\text{rot}} = \frac{1}{3} ; \quad \nu_{\text{ram}} = \frac{16}{3} ; \quad (20)$$

for homogeneous configurations with constant velocity on the equatorial plane, according to cases (b) and (c);

$$\eta_{\text{anm}} = 1 ; \quad \eta_{\text{rot}} = \frac{1}{2} ; \quad (21)$$

for rigidly rotating isopycnic surfaces, cases (a) and (c);

$$\eta_{\text{anm}} = \frac{3\pi}{8} ; \quad \eta_{\text{rot}} = \frac{3}{4} ; \quad (22)$$

for constant velocity everywhere, case (b). Further details can be found in CM03, CM05.

### 2.3 Virial equilibrium configurations

Let us define virial equilibrium as characterized by the validity of the virial theorem, and relaxed and unrelaxed configurations as systems where virial equilibrium does and does not coincide, respectively, with dynamical (or hydrostatic) equilibrium (CM05).

With regard to unrelaxed configurations, the generalized tensor virial equations read (CM05):

$$(E_{\text{sel}})_{pq} + 2(E_{\text{rot}})_{pq} + 2\zeta_{pq} E_{\text{pec}} = 0 ; \quad (23)$$

$$\zeta_{pq} = \frac{(\tilde{E}_{\text{pec}})_{pq}}{E_{\text{pec}}} ; \quad p = 1, 2, 3 ; \quad q = 1, 2, 3 ; \quad (24)$$

$$\sum_{p=1}^3 \zeta_{pp} = \frac{\tilde{E}_{\text{pec}}}{E_{\text{pec}}} = \zeta ; \quad 0 \leq \zeta_{pp} \leq \zeta ; \quad (25)$$

$$\zeta_{pq} = 0 ; \quad p \neq q ; \quad (26)$$

where  $\zeta_{pq}$  is the generalized anisotropy tensor,  $E_{\text{pec}}$  is the residual energy, and  $(\tilde{E}_{\text{pec}})_{pq} = \zeta_{pq}E_{\text{pec}}$  is the effective residual-energy tensor i.e. the right amount needed for the configuration of interest to be relaxed. The diagonal components of the generalized anisotropy tensor,  $\zeta_{pp}$ , may be conceived as generalized anisotropy parameters. The related trace,  $\zeta$ , may be conceived as a virial index, where  $\zeta = 1$  corresponds to null virial excess,  $2\Delta E_{\text{pec}} = 2(\tilde{E}_{\text{pec}} - E_{\text{pec}})$ , which does not necessarily imply a relaxed configuration<sup>5</sup>,  $\zeta > 1$  to positive virial excess, and  $\zeta < 1$  to negative virial excess.

The substitution of Eqs. (4)-(7) and (17)-(18) into the virial equations (23), and the particularization to the rotation axis,  $p = 3$ , allows the following expression of the peculiar energy (CM05):

$$E_{\text{pec}} = \frac{1}{2} \frac{GM^2}{a_1} \frac{\mathcal{S}_{33}}{\zeta_{33}} ; \quad (27)$$

accordingly, the remaining virial equations read (CM05):

$$(\zeta_{33}\mathcal{S}_{qq} - \zeta_{qq}\mathcal{S}_{33}) - 2h\zeta_{33}\mathcal{R}_{qq} = 0 ; \quad q = 1, 2 ; \quad (28)$$

$$h = \frac{J^2}{GM^3a_1} ; \quad (29)$$

where  $h$  may be conceived as a rotation parameter. It is apparent that Eq. (28) admits real solutions provided the following inequalities hold:

$$\frac{\zeta_{qq}}{\zeta_{33}} \leq \frac{\mathcal{S}_{qq}}{\mathcal{S}_{33}} ; \quad q = 1, 2 ; \quad (30)$$

which is the natural extension of its counterpart related to axisymmetric, relaxed configurations (Wiegandt 1982a,b).

## 2.4 Rotation and anisotropy parameters

To get a more evident connection with the centrifugal potential on the boundary, let us define the rotation parameter (CM05):

$$v = \frac{\Omega^2}{2\pi G\bar{\rho}} ; \quad (31)$$

---

<sup>5</sup>For instance, a homogeneous sphere undergoing coherent oscillations exhibits  $\zeta > 1$  at expansion turnover and  $\zeta < 1$  at contraction turnover. Then it necessarily exists a configuration where  $\zeta = 1$  which, on the other hand, is unrelaxed.

where  $\Omega = \Omega(a_1, 0, 0)$  is the angular velocity at the end of the major equatorial semiaxis, denoted as  $a_1$ , and  $\bar{\rho}$  is the mean density of the ellipsoid:

$$\bar{\rho} = \frac{3}{4\pi} \frac{M}{a_1 a_2 a_3} ; \quad (32)$$

the above definition of the rotation parameter,  $v$ , makes a generalization of some special cases mentioned in the literature (e.g., Jeans 1929, Chap. IX, §232; Chandrasekhar & Lebovitz 1962).

The combination of Eqs. (15), (29), (31), and (32) yields:

$$h = \frac{3}{2} \eta_{\text{anm}}^2 \nu_{\text{anm}}^2 \frac{(1 + \epsilon_{21}^2)^2}{\epsilon_{21} \epsilon_{31}} v ; \quad (33)$$

which links the rotation parameters,  $h$  and  $v$ . An explicit expression of the rotation parameter,  $h$ , may directly be obtained from Eq. (28), as:

$$h = \frac{1}{2} \frac{\zeta_{33} \mathcal{S}_{qq} - \zeta_{qq} \mathcal{S}_{33}}{\zeta_{33} \mathcal{R}_{qq}} ; \quad q = 1, 2 ; \quad (34)$$

and the substitution of Eqs. (34) into (33), using (17) and (18), allows the explicit expression of the rotation parameter,  $v$ , as:

$$v = \frac{1}{3} \frac{\epsilon_{21} \epsilon_{31}}{(1 + \epsilon_{21}^2)^2} \frac{1}{\eta_{\text{anm}}^2 \nu_{\text{anm}}^2} \frac{\zeta_{33} \mathcal{S}_{qq} - \zeta_{qq} \mathcal{S}_{33}}{\zeta_{33} \mathcal{R}_{qq}} ; \quad q = 1, 2 ; \quad (35)$$

which, in the special case of rigidly rotating, homogeneous configurations with isotropic peculiar velocity distribution, reduces to a known relation for Jacobi ellipsoids and, with the additional demand of axial symmetry, to a known relation for MacLaurin spheroids (e.g., Jeans 1929, Chap. VIII, §§189-193; Chandrasekhar 1969, Chap. 5, §32, Chap. 6, §39; Caimmi 1996a).

An explicit expression of anisotropy parameter ratio, can be obtained via Eq. (34). The result is (CM05):

$$\frac{\zeta_{qq}}{\zeta_{33}} = \frac{\mathcal{S}_{qq}}{\mathcal{S}_{33}} \left[ 1 - 2h \frac{\mathcal{R}_{qq}}{\mathcal{S}_{qq}} \right] ; \quad q = 1, 2 ; \quad (36)$$

$$\frac{\zeta_{11}}{\zeta_{22}} = \frac{\mathcal{S}_{11} - 2h \mathcal{R}_{11}}{\mathcal{S}_{22} - 2h \mathcal{R}_{22}} ; \quad (37)$$

and the combination of Eqs. (25) and (36) yields:

$$\frac{\zeta_{33}}{\zeta} = \frac{\mathcal{S}_{33}}{\mathcal{S} - 2h\mathcal{R}} ; \quad (38)$$

which provides an alternative expression to Eqs. (34) and (35), as (C06):

$$h = \frac{1}{2} \frac{\zeta_{33}\mathcal{S} - \zeta\mathcal{S}_{33}}{\zeta_{33}\mathcal{R}} ; \quad (39)$$

$$v = \frac{1}{3} \frac{\epsilon_{21}\epsilon_{31}}{(1 + \epsilon_{21}^2)^2} \frac{1}{\eta_{amn}^2 \nu_{amn}^2} \frac{\zeta_{33}\mathcal{S} - \zeta\mathcal{S}_{33}}{\zeta_{33}\mathcal{R}} ; \quad (40)$$

that are equivalent to Eq. (28), and then admit real solutions provided inequality (30) is satisfied.

Finally, Eqs. (28) may be combined as:

$$\frac{\mathcal{R}_{11}}{\mathcal{R}_{22}} = \frac{\zeta_{33}\mathcal{S}_{11} - \zeta_{11}\mathcal{S}_{33}}{\zeta_{33}\mathcal{S}_{22} - \zeta_{22}\mathcal{S}_{33}} ; \quad (41)$$

where it can be seen that Eqs. (37) and (41) are changed one into the other, by replacing the terms,  $\mathcal{S}_{33}\zeta_{qq}/\zeta_{33}$ , with the terms,  $2h\mathcal{R}_{qq}$ , and vice versa.

In the special case of axisymmetric configurations, the shape factors related to equatorial axes coincide,  $A_2 = A_1$ , as  $\epsilon_{21} = 1$  (e.g., CM05). Then  $\mathcal{S}_{11} = \mathcal{S}_{22}$  owing to Eqs. (6), (7), and  $\mathcal{R}_{11} = \mathcal{R}_{22}$  owing to Eqs. (17), which necessarily imply  $\zeta_{11} = \zeta_{22}$ , owing to Eq. (41).

In the general case of triaxial configurations, the contrary holds,  $A_2 \neq A_1$ , as  $\epsilon_{21} \neq 1$ , then  $\mathcal{S}_{11} \neq \mathcal{S}_{22}$  and  $\mathcal{R}_{11} \neq \mathcal{R}_{22}$ , then the equality,  $\zeta_{11} = \zeta_{22}$ , via Eq. (37), implies the validity of the relation:

$$h = \frac{1}{2} \frac{\mathcal{S}_{11} - \mathcal{S}_{22}}{\mathcal{R}_{11} - \mathcal{R}_{22}} ; \quad (42)$$

if otherwise, the residual velocity distribution along the equatorial plane<sup>6</sup> is anisotropic i.e.  $\zeta_{11} \neq \zeta_{22}$ . The related degeneracy can be removed using an additional condition, as it will be shown in the next section.

---

<sup>6</sup>Throughout this paper, “along the equatorial plane” has to be intended as “along any direction parallel to the equatorial plane”.

### 3 A unified theory of systematic and random motions

#### 3.1 Imaginary rotation

A unified theory of systematic and random motions is allowed, taking into consideration imaginary rotation, as discussed in earlier attempts (Caimmi 1993b; C06), and an interested reader is addressed therein for deeper insight. What is relevant for the current investigation, shall be mentioned and further developed here.

It has been shown above that Eq. (28), or equivalently one among (34), (35), (39), (40), admits real solutions provided inequality (30) is satisfied. If otherwise, the rotation parameter - let it be  $h$  or  $v$  - has necessarily to be negative, which implies, via Eqs. (29) or (31), an *imaginary* angular velocity,  $i\Omega$ , where  $i$  is the imaginary unit. Accordingly, the centrifugal potential takes the general expression (C06):

$$\mathcal{T}^\mp(x_1, x_2, x_3) = \mp \frac{1}{2} [\Omega(x_1, x_2, x_3)]^2 w^2 ; \quad w^2 = x_1^2 + x_2^2 ; \quad (43)$$

where the minus and the plus correspond to imaginary and real rotation, respectively. The centrifugal force related to real rotation,  $\partial\mathcal{T}^+/\partial w$ , has opposite sign with respect to the gravitational force,  $\partial\mathcal{V}/\partial w$ . On the other hand, the centrifugal force related to imaginary rotation,  $\partial\mathcal{T}^-/\partial w$ , has equal sign with respect to the gravitational force,  $\partial\mathcal{V}/\partial w$ . Then the net effect of real rotation is flattening, while the net effect of imaginary rotation is *elongation*, with respect to the rotation axis (Caimmi 1996b).

To get further insight, let us particularize Eq. (28) to the special case of null rotation ( $h = 0$ ). The result is:

$$\frac{\zeta_{qq}}{\zeta_{33}} = \frac{\mathcal{S}_{qq}}{\mathcal{S}_{33}} ; \quad h = 0 ; \quad q = 1, 2 ; \quad (44)$$

where the right-hand side, via Eqs. (6) and (7), depends on the axis ratios only. It can be seen (Appendix A) that  $\mathcal{S}_{qq}/\mathcal{S}_{33} \geq 1$  for oblate-like configurations ( $a_1 \geq a_2 \geq a_3$ ), and  $\mathcal{S}_{qq}/\mathcal{S}_{33} \leq 1$  for prolate-like configurations ( $a_2 \leq a_1 \leq a_3$ ), which implies  $\zeta_{qq}/\zeta_{33} \geq 1$  for oblate-like configurations, and  $\zeta_{qq}/\zeta_{33} \leq 1$  for prolate-like configurations. Accordingly, the net effect

of positive or negative residual motion excess along the equatorial plane is flattening or elongation, respectively. In what follows, it shall be intended that residual motion excess is related to the equatorial plane.

### 3.2 Residual motion excess and rotation

With regard to the rotation parameter,  $v$ , it is convenient to use the more compact notation<sup>7</sup> (C06):

$$v_N = \frac{3\eta_{\text{rot}}\nu_{\text{rot}}}{\nu_{\text{sel}}} v ; \quad (45)$$

and the substitution of Eqs. (6), (7), (17), (18), into (35) and (40), yields the equivalent expressions:

$$v_N = A_q - \frac{\zeta_{qq}}{\zeta_{33}} \epsilon_{3q}^2 A_3 ; \quad q = 1, 2 ; \quad (46)$$

$$v_N = \frac{1}{1 + \epsilon_{21}^2} \left[ A_1 + \epsilon_{21}^2 A_2 + \frac{\zeta_{33} - \zeta}{\zeta_{33}} \epsilon_{31}^2 A_3 \right] ; \quad (47)$$

which shows that, for homeoidally striated Jacobi ellipsoids, the normalized rotation parameter,  $v_N$ , depends on the axis ratios,  $\epsilon_{21}$ ,  $\epsilon_{31}$ , and a *single* anisotropy parameter,  $\tilde{\zeta}_{33} = \zeta_{33}/\zeta$ . In the special case of homogeneous, rigidly rotating configurations, owing to Eqs. (10b), (19), and (21), Eq. (45) reduces to:  $v_N = v$ .

In the limit of isotropic residual velocity distribution,  $\zeta_{11} = \zeta_{22} = \zeta_{33} = \zeta/3$ , Eqs. (46) and (47) take the simpler form (C06):

$$(v_N)_{\text{iso}} = A_q - \epsilon_{3q}^2 A_3 ; \quad q = 1, 2 ; \quad (48)$$

$$(v_N)_{\text{iso}} = \frac{1}{1 + \epsilon_{21}^2} \left[ A_1 + \epsilon_{21}^2 A_2 - 2\epsilon_{31}^2 A_3 \right] ; \quad (49)$$

where the index, iso, means isotropic residual velocity distribution.

Accordingly, Eqs. (46) and (47) may be expressed as (C06):

$$v_N = (v_N)_{\text{iso}} - (v_N)_{\text{ani}} ; \quad (50)$$

---

<sup>7</sup>The factor, 3, does not appear in CM05:  $v_N = 3(v_N)_{\text{CM05}}$ . The current normalization is more convenient in dealing with a general theory (Caimmi, in preparation).

$$(v_N)_{\text{ani}} = \left( \frac{\zeta_{qq}}{\zeta_{33}} - 1 \right) \epsilon_{3q}^2 A_3 ; \quad (51)$$

$$(v_N)_{\text{ani}} = \left( \frac{\zeta}{\zeta_{33}} - 3 \right) \frac{\epsilon_{31}^2 A_3}{1 + \epsilon_{21}^2} ; \quad (52)$$

where  $(v_N)_{\text{ani}} \geq 0$  for oblate-like configurations,  $\zeta_{qq}/\zeta_{33} \geq 1$ ;  $(v_N)_{\text{ani}} \leq 0$  for prolate-like configurations,  $\zeta_{qq}/\zeta_{33} \leq 1$ ; and the index,  $\text{ani}$ , means contribution from residual motion excess. Accordingly, positive residual motion excess is related to real rotation. On the contrary, negative residual motion excess is related to imaginary rotation.

Let us rewrite Eq. (50) as:

$$(v_N)_{\text{iso}} = v_N + (v_N)_{\text{ani}} ; \quad (53)$$

which, owing to Eqs. (31) and (45), is equivalent to:

$$\Omega_{\text{iso}}^2 = \Omega^2 \mp \Omega_{\text{ani}}^2 ; \quad (54)$$

where the plus corresponds to real rotation,  $(v_N)_{\text{ani}} \geq 0$ , and the minus to imaginary rotation,  $(v_N)_{\text{ani}} \leq 0$ . Then the effect of residual motion excess on the shape of the system, is virtually indistinguishable from the effect of additional systematic rotation, with similar (rotation) velocity distribution as the pre-existing one. The related, explicit expression, according to Eqs. (12), (31), and (52), is (C06):

$$\frac{\Omega_{\text{ani}}(r, \theta)}{\Omega_{\text{ani}}(R, \theta)} = \frac{\Omega_{\text{ani}}(a'_1, 0)}{\Omega_{\text{ani}}(a_1, 0)} = \frac{\Omega(a'_1, 0)}{\Omega(a_1, 0)} = \frac{\Omega(r, \theta)}{\Omega(R, \theta)} ; \quad (55)$$

$$\Omega_{\text{ani}}^2 = \Omega_{\text{ani}}^2(a_1) = \mp (v_N)_{\text{ani}} \frac{\nu_{\text{sel}}}{3\eta_{\text{rot}}\nu_{\text{rot}}} 2\pi G \bar{\rho} ; \quad (56)$$

where the double sign ensures a non negative value on the right hand-side member of Eq. (56). Accordingly, a homeoidally striated Jacobi ellipsoid with assigned systematic rotation and residual velocity distribution, with regard to the shape, is virtually indistinguishable from an adjoint configuration of equal mass and axes, systematic rotation velocity distribution deduced from Eqs. (12), (55) and (56), and isotropic residual velocity distribution.

Owing to Eqs. (50), (51), and (52), Eqs. (48) and (49) are equivalent to (46) and (47), respectively. On the other hand, Eqs. (48) and (49) are valid for classical Jacobi ellipsoids with rotation parameter,  $v = (v_N)_{\text{iso}}$ .

Accordingly, a homeoidally striated Jacobi ellipsoid (in general, an unrelaxed configuration) with assigned systematic rotation and residual velocity distribution, with regard to the shape, is virtually indistinguishable from an adjoint, classical Jacobi ellipsoid (a relaxed configuration) of equal mass and axes, and rotation parameter equal to the normalized rotation parameter of the original configuration.

### 3.3 Axis ratios and anisotropy parameters

The combination of the alternative expressions of the rotation parameter,  $(v_N)_{\text{iso}}$ , expressed by Eqs. (48), yields:

$$\epsilon_{21}^2 (A_2 - A_1) = (1 - \epsilon_{21}^2) \epsilon_{31}^2 A_3 ; \quad (57)$$

which, for axisymmetric configurations, reduces to an indeterminate form,  $0 = 0$ .

The combination of the alternative expressions of the rotation parameter,  $(v_N)_{\text{ani}}$ , expressed by Eqs. (51), yields:

$$\zeta_{33} - \zeta_{22} = \epsilon_{21}^2 (\zeta_{33} - \zeta_{11}) ; \quad (58)$$

which, for isotropic residual velocity distributions, reduces to an indeterminate form,  $0 = 0$ . In addition, axisymmetric configurations ( $\epsilon_{21} = 1$ ) necessarily imply isotropic residual velocity distributions along the equatorial plane,  $\zeta_{11} = \zeta_{22}$ .

The combination of Eqs. (25) and (58) yields:

$$\zeta_{11} = \frac{\zeta - (2 - \epsilon_{21}^2) \zeta_{33}}{1 + \epsilon_{21}^2} ; \quad (59a)$$

$$\zeta_{22} = \frac{\epsilon_{21}^2 \zeta + (1 - 2\epsilon_{21}^2) \zeta_{33}}{1 + \epsilon_{21}^2} ; \quad (59b)$$

which, for axisymmetric configurations ( $\epsilon_{21} = 1$ ) reduces to  $\zeta_{11} = \zeta_{22} = (\zeta - \zeta_{33})/2$ , and the special case,  $\zeta_{33} = \zeta/3$ , reads  $\zeta_{11} = \zeta_{22} = \zeta/3$ .

The condition,  $\zeta_{11} \geq 0$ , related to Eqs. (24), necessarily implies  $0 \leq \zeta_{33}/\zeta \leq 1/2$  for  $\epsilon_{21} = 0$ . If otherwise, sequences of virial equilibrium configurations cannot attain the oblong shape,  $\epsilon_{21} = \epsilon_{31} = 0$ , but must stop earlier, where the equivalent relations:

$$\epsilon_{21}^2 = \frac{2\zeta_{33} - \zeta}{\zeta_{33}} ; \quad \zeta_{11} = 0 ; \quad (60)$$

are satisfied.

Accordingly, with regard to homeoidally striated Jacobi ellipsoids, the anisotropy parameters along the equatorial plane,  $\zeta_{11}$  and  $\zeta_{22}$ , cannot be arbitrarily assigned, but depend on the equatorial axis ratio,  $\epsilon_{21}$ , conform to Eqs. (59). On the other hand, the further knowledge of the meridional axis ratio,  $\epsilon_{31}$ , and the rotation parameter,  $v_N$ , allows the determination of the rotation parameter,  $(v_N)_{\text{ani}}$ , via Eqs. (48), (49), (50), and then the ratios,  $\zeta_{qq}/\zeta_{33}$ ,  $\zeta_{33}/\zeta$ , via Eqs. (51), (52), respectively, or the anisotropy parameter along the rotation axis,  $\zeta_{33}$ , provided the virial index,  $\zeta$ , defined by Eq. (25), is assigned.

In conclusion, with regard to homeoidally striated Jacobi ellipsoids defined by assigned axis ratios,  $\epsilon_{31}$ ,  $\epsilon_{21}$ , rotation parameter,  $v_N$ , and virial index,  $\zeta$ , the anisotropy parameters,  $\zeta_{11}$ ,  $\zeta_{22}$ ,  $\zeta_{33}$ , cannot arbitrarily be fixed, but must be determined as shown above.

### 3.4 Centrifugal support along the major equatorial axis

The calculation of the gravitational force, induced by homeoidally striated Jacobi ellipsoids, involves numerical integrations (e.g., Chandrasekhar 1969, Chap. 3, § 20) and is outside the aim of the current paper. With regard to an assigned isopycnic surface internal to, or coinciding with, the boundary, the gravitational force,  $F_G$ , induced at the end of the related major equatorial semiaxis,  $a'_1$ , satisfies the inequality:

$$-[F_G(a'_1, 0, 0)]_{\text{sph}} \leq -F_G(a'_1, 0, 0) \leq -[F_G(a'_1, 0, 0)]_{\text{foc}} ;$$

where the left-hand side is related to spherical isopycnics with unchanged major equatorial axes, and the right-hand side to confocal isopycnic surfaces from the one under consideration to the centre. Owing to the Newton's and MacLaurin's theorem (e.g., Caimmi 2003), the following relations hold:

$$F_G(a'_1, 0, 0) = -2\pi G \bar{\rho}_{\text{xxx}}(a'_1) (A_1)_{\text{xxx}} a'_1 ; \quad (61)$$

where  $\bar{\rho}(a'_1)$  is the mean density within the isopycnic surface, and  $\text{xxx} = \text{sph}, \text{foc}$ , for the striated sphere and the focaloidally striated ellipsoid surrounded by the homeoidally striated corona, respectively.

The balance between gravitational and centrifugal force at the end of the major equatorial axis of the isopycnic surface under discussion, reads:

$$-2\pi G \bar{\rho}_{\text{xxx}}(a'_1) (A_1)_{\text{xxx}} a'_1 + \Omega_{\text{iso}}^2(a'_1) a'_1 = 0 ; \quad (62)$$

where the angular velocity,  $\Omega_{\text{iso}}$ , takes into account both systematic rotation and residual motion excess, according to Eq. (54). On the other hand, the generalization of Eq. (31) to a generic isopycnic surface within the boundary, reads:

$$v(a'_1) = \frac{\Omega^2(a'_1)}{2\pi G \bar{\rho}_{\text{xxx}}(a'_1)} ; \quad (63)$$

and the combination of Eqs. (45), (53), (54), (62), (63), yields:

$$\{[v_{\text{iso}}(a'_1)]_{\text{eq}}\}_{\text{xxx}} = \frac{\Omega_{\text{iso}}^2(a'_1)}{2\pi G \bar{\rho}_{\text{xxx}}(a'_1)} = (A_1)_{\text{xxx}} ; \quad (64)$$

where the index,  $\text{eq}$ , denotes the rotation parameter,  $v_{\text{iso}}(a'_1)$ , related to centrifugal support at the end of major equatorial axis of the isopycnic surface under consideration. The above results allow the validity of the relation:

$$\{[v_{\text{iso}}(a'_1)]_{\text{eq}}\}_{\text{cof}} \leq [v_{\text{iso}}(a'_1)]_{\text{eq}} \leq \{[v_{\text{iso}}(a'_1)]_{\text{eq}}\}_{\text{sph}} ; \quad (65)$$

where  $[v_{\text{iso}}(a'_1)]_{\text{eq}}$  is the critical value related to the homeoidally striated Jacobi ellipsoid, with regard to an assigned isopycnic surface internal to, or coinciding with, the boundary. Then  $v_{\text{iso}}(a'_1) \geq \{[v_{\text{iso}}(a'_1)]_{\text{eq}}\}_{\text{cof}}$  and  $v_{\text{iso}}(a'_1) \leq \{[v_{\text{iso}}(a'_1)]_{\text{eq}}\}_{\text{sph}}$  make a sufficient and a necessary condition, respectively, for the occurrence of centrifugal support at the end of major equatorial axis in the case under consideration.

Owing to the Newton's and MacLaurin's theorem, the condition of centrifugal support, Eq. (64), for focaloidally striated ellipsoids surrounded by homeoidally striated coronae, coincides with its counterpart related to homogeneous ellipsoids with equal mean density, axis ratios, and velocity field. On the other hand, the rotation parameter,  $v_{\text{iso}}(a'_1)$ , in the special case of focaloidally striated ellipsoids, is also expressed by Eq. (64), particularized to classical Jacobi ellipsoids. A comparison with the last part of Eq. (64) shows that centrifugal support in focaloidally striated ellipsoids occurs only for flat configurations,  $\epsilon_{31} = 0$ . Accordingly, Eq. (65) reduces to:

$$0 \leq [v_{\text{iso}}(a'_1)]_{\text{eq}} \leq \frac{2}{3} ; \quad (66)$$

owing to Eq. (64) and  $(A_1)_{\text{sph}} = 2/3$  (e.g., CM03).

With regard to rigid rotation, it is a well known result that the occurrence of centrifugal support, at the end of the major equatorial axis, depends on

the steepness of the density profile (e.g., Jeans 1929, Chap. IX, §§ 230-240). More precisely, a steeper density profile implies an earlier centrifugal support and vice versa, unless the bifurcation point from ellipsoidal to pear-shaped configurations is attained, which occurs for nearly homogeneous matter distributions. A similar trend is expected to hold for any velocity profile of the kind considered in the current paper.

The combination of Eq. (65) with its counterpart related to the boundary, yields:

$$v_{\text{iso}}(a'_1) = v_{\text{iso}} \frac{M}{M(a'_1)} \left( \frac{a'_1}{a_1} \right)^3 \frac{\Omega^2(a'_1)}{\Omega^2(a_1)} ; \quad (67)$$

a further restriction to mass distributions obeying the following law:

$$\frac{M(a'_1)}{M} = \left( \frac{a'_1}{a_1} \right)^k ; \quad 0 \leq k \leq 3 ; \quad (68)$$

where  $k = 3, 1, 0$ , represent homogeneous, isothermal, and Roche-like mass distributions, make Eq. (67) reduce to:

$$v_{\text{iso}}(a'_1) = v_{\text{iso}} \left( \frac{a'_1}{a_1} \right)^{3-k} \frac{\Omega^2(a'_1)}{\Omega^2(a_1)} ; \quad (69)$$

where the last factor equals unity for rigid rotation and the ratio,  $(a_1/a'_1)^2$ , for constant velocity along the major equatorial axis. Accordingly, centrifugal support at the end of major equatorial axis is first attained on the boundary in the former alternative,  $v_{\text{iso}}(a'_1) \leq v_{\text{iso}}(a_1)$ .

In the latter alternative, Eq. (69) reduces to:

$$v_{\text{iso}}(a'_1) = v_{\text{iso}} \left( \frac{a'_1}{a_1} \right)^{1-k} ; \quad (70)$$

which, for sufficiently steep density profiles,  $0 \leq k \leq 1$ , shows a similar trend with respect to the former alternative. On the other hand, centrifugal support is first attained everywhere along the major equatorial axis for isothermal mass distributions,  $k = 1$ , and at the centre for sufficiently mild density profiles,  $1 \leq k \leq 3$ , which implies  $v_{\text{iso}}(a'_1) \geq v_{\text{iso}}(a_1)$ .

The combination of Eqs. (45) and (64) yields:

$$\{[(v_N)_{\text{iso}}(a'_1)]_{\text{eq}}\}_{\text{xxx}} = \frac{3\eta_{\text{rot}}\nu_{\text{rot}}}{\nu_{\text{sel}}} (A_1)_{\text{xxx}} ; \quad (71)$$

and Eq. (66) reads:

$$0 \leq [(v_N)_{\text{iso}}(a'_1)]_{\text{eq}} \leq \frac{2\eta_{\text{rot}}\nu_{\text{rot}}}{\nu_{\text{sel}}} ; \quad (72)$$

in terms of the normalized rotation parameter,  $v_N$ .

### 3.5 Bifurcation points

Given a homeidally striated ellipsoid, it has been shown above (see also C06) that the adjoint configuration, characterized by isotropic peculiar velocity distribution and normalized rotation parameter,  $(v_N)_{\text{iso}}$ , exhibits same shape as a classical Jacobi ellipsoid of equal mass and axes, in real or imaginary rotation, where  $v = (v_N)_{\text{iso}}$ . Accordingly, the bifurcation point from axisymmetric to triaxial configurations is related to an axis ratio,  $\epsilon_{31}$ , which is independent of the amount of systematic rotation and residual motion excess, conform to Eq. (53). To gain more insight, let us equalize the alternative expressions of Eq. (46). The result is:

$$A_1 - \frac{\zeta_{11}}{\zeta_{33}}\epsilon_{31}^2 A_3 = A_2 - \frac{\zeta_{22}}{\zeta_{33}}\epsilon_{32}^2 A_3 ; \quad (73)$$

and the combination of Eqs. (59) and (73) yields:

$$\frac{A_2 - A_1}{1 - \epsilon_{21}^2} = \frac{\epsilon_{31}^2}{\epsilon_{21}^2} A_3 ; \quad (74)$$

then the bifurcation points occur at a configuration, where the axis ratio,  $\epsilon_{31}$ , is the solution of the transcendental equation (Caimmi 1996a):

$$\lim_{\epsilon_{21} \rightarrow 1} \epsilon_{21}^2 \frac{A_2 - A_1}{1 - \epsilon_{21}^2} = \epsilon_{31}^2 A_3 ; \quad (75)$$

where Eqs. (74) and (75) coincide with their counterparts related to isotropic residual velocity distributions (Caimmi 1996a,b).

The contradiction with earlier results (Wiegandt 1982a,b; CM05) is explained in the following way. Let us suppose that the generalized anisotropy parameters,  $\zeta_{11}, \zeta_{22}, \zeta_{33}$ , can be arbitrarily fixed regardless from Eqs. (59),

and assume  $\zeta_{11} = \zeta_{22}$  *also* for triaxial configurations. Accordingly, Eq. (73) reads:

$$\frac{A_2 - A_1}{1 - \epsilon_{21}^2} = \frac{\zeta_{11} \epsilon_{31}^2}{\zeta_{33} \epsilon_{21}^2} A_3 ; \quad (76)$$

and the bifurcation points occur at a configuration where the axis ratio,  $\epsilon_{31}$ , is the solution of the transcendental equation:

$$\lim_{\epsilon_{21} \rightarrow 1} \epsilon_{21}^2 \frac{A_2 - A_1}{1 - \epsilon_{21}^2} = \frac{\zeta_{11}}{\zeta_{33}} \epsilon_{31}^2 A_3 ; \quad (77)$$

which coincides with Wiegandt (1982b) criterion for bifurcation, with regard to homeoidally striated Jacobi ellipsoids in rigid rotation. For a formal demonstration, see Appendix B. Then Wiegandt's criterion for bifurcation, expressed by Eq. (77), is in contradiction with Eqs. (59), contrary to the current one, expressed by Eq. (75).

## 4 Transitions from and towards homeoidally striated Jacobi ellipsoids

In a classical paper, Thuan & Gott (1975) modelled virialized elliptical galaxies and related progenitor density perturbations at turn around as MacLaurin spheroids and rigidly rotating homogeneous spheres, respectively, and found a relation between the initial ratio of rotation to potential energy and the final shape. Surprisingly, the model succeeded in explaining why elliptical galaxies more flattened than  $E7$  cannot exist.

In a recent attempt (CM05) the above mentioned procedure has been generalized passing from MacLaurin spheroids to homeoidaly striated Jacobi ellipsoids, and the interested reader is addressed therein for deeper insight. What is relevant for the current investigation, shall be mentioned and further developed here.

Let the initial and the final configuration be homeoidaly striated Jacobi ellipsoids, and let the former be denoted by a prime. The identity:

$$E_{\text{rot}} = \frac{E_{\text{rot}}}{E'_{\text{rot}}} \frac{E'_{\text{rot}}}{E'_{\text{sel}}} \frac{E'_{\text{sel}}}{E_{\text{sel}}} (-E_{\text{sel}}) ;$$

owing to Eqs. (5) and (18a), may be cast under the equivalent form (CM05):

$$\frac{a'_1}{a_1} = \frac{\beta_M^3}{\beta_J^2} \frac{\mathcal{S}}{\mathcal{S}'} \frac{\mathcal{R}'}{\mathcal{R}} \frac{\mathcal{E}_{\text{rot}}}{\mathcal{E}'_{\text{rot}}} ; \quad (78\text{a})$$

$$\beta_J = \frac{J}{J'} ; \quad \beta_M = \frac{M}{M'} \quad \mathcal{E}_{\text{rot}} = -\frac{E_{\text{rot}}}{E_{\text{sel}}} ; \quad (78\text{b})$$

involving dimensionless quantities only.

On the other hand, the identity:

$$\begin{aligned} E &= E_{\text{sel}} + E_{\text{rot}} + E_{\text{res}} = \frac{E}{E'} E' \\ &= \frac{E}{E'} (E'_{\text{sel}} + E'_{\text{rot}} + E'_{\text{pec}} + E'_{\text{osc}}) ; \end{aligned}$$

by use of Eqs. (23), and (26), may be cast under the equivalent form (CM05):

$$\begin{aligned} \frac{E_{\text{sel}}}{E'_{\text{sel}}} - \mathcal{E}_{\text{rot}} \frac{E_{\text{sel}}}{E'_{\text{sel}}} - \frac{1}{2\zeta} \frac{E_{\text{sel}}}{E'_{\text{sel}}} + \frac{1}{\zeta} \frac{E_{\text{sel}}}{E'_{\text{sel}}} \mathcal{E}_{\text{rot}} \\ = \beta_E (1 - \mathcal{E}'_{\text{rot}} - \mathcal{E}'_{\text{pec}} - \mathcal{E}'_{\text{osc}}) ; \end{aligned} \quad (79\text{a})$$

$$\beta_E = \frac{E}{E'} ; \quad \mathcal{E}_{\text{rot}} = -\frac{E_{\text{rot}}}{E_{\text{sel}}} ; \quad \mathcal{E}_{\text{pec}} = -\frac{E_{\text{pec}}}{E_{\text{sel}}} ;$$

$$\mathcal{E}_{\text{osc}} = -\frac{E_{\text{osc}}}{E_{\text{sel}}} ; \quad (79\text{b})$$

$$\zeta = -\frac{E_{\text{sel}} + 2E_{\text{rot}}}{2(E_{\text{osc}} + E_{\text{pec}})} ; \quad (79\text{c})$$

where  $E_{\text{osc}}$ ,  $E_{\text{pec}}$ , represent the kinetic energy of systematic radial and non systematic motions, respectively.

The combination of Eqs. (5), (18a), and (79) yields after some algebra:

$$\begin{aligned} \beta_M^2 \frac{\mathcal{S}}{\mathcal{S}'} \frac{a'_1}{a_1} \left[ \frac{2\zeta - 1}{2\zeta} - \frac{\zeta - 1}{\zeta} \mathcal{E}_{\text{rot}} \right] \\ - \beta_E (1 - \mathcal{E}'_{\text{rot}} - \mathcal{E}'_{\text{pec}} - \mathcal{E}'_{\text{osc}}) = 0 ; \end{aligned} \quad (80)$$

involving dimensionless quantities only.

The substitution of Eq. (78a) into (80) produces a second-degree equation in  $\mathcal{E}'_{\text{rot}}$ , as (CM05):

$$\mathcal{E}'_{\text{rot}}^2 - 2b\mathcal{E}'_{\text{rot}} + c = 0 ; \quad (81\text{a})$$

$$b = \frac{1}{2} (1 - \mathcal{E}'_{\text{osc}} - \mathcal{E}'_{\text{pec}}) ; \quad (81\text{b})$$

$$c = \frac{\beta_M^5}{\beta_J^2 \beta_E} \left( \frac{\mathcal{S}}{\mathcal{S}'} \right)^2 \frac{\mathcal{R}'}{\mathcal{R}} \mathcal{E}_{\text{rot}} \left[ \frac{2\zeta - 1}{2\zeta} - \frac{\zeta - 1}{\zeta} \mathcal{E}_{\text{rot}} \right] ; \quad (81\text{c})$$

the (reduced) discriminant of this equation is (CM05):

$$\Delta = b^2 - \frac{\beta_M^5}{\beta_J^2 \beta_E} \left( \frac{\mathcal{S}}{\mathcal{S}'} \right)^2 \frac{\mathcal{R}'}{\mathcal{R}} \mathcal{E}_{\text{rot}} \left[ \frac{2\zeta - 1}{2\zeta} - \frac{\zeta - 1}{\zeta} \mathcal{E}_{\text{rot}} \right] ; \quad (82)$$

with regard to a transition from an initial to a final configuration, where all the parameters which appear in Eq. (82) are specified, except the axis ratios,  $\epsilon_{21}$  and  $\epsilon_{31}$ . The condition,  $\Delta = 0$ , via Eq. (82), represents a curve in the  $(\mathcal{O}\epsilon_{21}\epsilon_{31})$  plane. The transition is forbidden for all values of the axis ratios, which make a negative discriminant, and then imaginary solutions.

The solutions of Eq. (81a) are:

$$\mathcal{E}'_{\text{rot}} = b \mp \left\{ b^2 - \frac{\beta_M^5}{\beta_J^2 \beta_E} \left( \frac{\mathcal{S}}{\mathcal{S}'} \right)^2 \frac{\mathcal{R}'}{\mathcal{R}} \mathcal{E}_{\text{rot}} \times \left[ \frac{2\zeta - 1}{2\zeta} - \frac{\zeta - 1}{\zeta} \mathcal{E}_{\text{rot}} \right] \right\}^{1/2} ; \quad (83)$$

and the combination of Eqs. (78a) and (83) yields:

$$\frac{a_1}{a'_1} = \frac{\beta_J^2}{\beta_M^3} \frac{\mathcal{S}'}{\mathcal{S}} \frac{\mathcal{R}}{\mathcal{R}'} \frac{1}{\mathcal{E}_{\text{rot}}} \left\{ b \mp \left[ b^2 - \frac{\beta_M^5}{\beta_J^2 \beta_E} \left( \frac{\mathcal{S}}{\mathcal{S}'} \right)^2 \frac{\mathcal{R}'}{\mathcal{R}} \mathcal{E}_{\text{rot}} \times \left( \frac{2\zeta - 1}{2\zeta} - \frac{\zeta - 1}{\zeta} \mathcal{E}_{\text{rot}} \right) \right]^{1/2} \right\} ; \quad (84)$$

where the rotation parameter,  $\mathcal{E}'_{\text{rot}}$ , and the axis ratio,  $a_1/a'_1$ , are left unchanged for different departures from mass, angular momentum, and energy conservation, provided the ratios:

$$\beta_{\mathcal{E}} = \frac{\beta_M^5}{\beta_J^2 \beta_E} ; \quad \beta_a = \frac{\beta_J^2}{\beta_M^3} ; \quad (85)$$

do not vary.

## 5 The ending point of the sequence of elliptical galaxies

The results of the current paper allow an extension and a generalization of the classical physical interpretation of the Hubble (1926) sequence (e.g., Jeans 1929, Chap. XIII, §§ 298-303) to anisotropic peculiar velocity distributions. Owing to the results of Sect. 3, it will suffice to restrict to solid-body rotating configurations with isotropic peculiar velocity distributions, but with imaginary rotation also taken into consideration.

### 5.1 Classification of galaxies

It is worth recalling that, before establishing their similarity to the Milky Way, galaxies were referred to as “great nebulae” or “nebulae”. In the words of Jeans (1929, Chap. XIII, § 298):

“Hubble finds that it is not possible to place all observed nebulae in one continuous sequence; their proper representation demands a Y-shaped diagram. (...)

The lower half of the Y is formed by nebulae of approximately elliptical or circular shape. These are subdivided into eight classes, designated  $E0, E1, \dots, E7$ , the numerical index being the integer nearest to  $10[(a-b)/a]$ , where  $a$  and  $b$  are the greatest and the least diameter of the nebulae as projected on the sky. Thus  $E0$  consists of nearly circular nebulae ( $b > 0.95a$ ), while  $E7$  consists of nebulae for which  $b$  is about  $0.3a$ , this being the greatest inequality of axes observed in the “elliptical” nebulae. (...)

The upper half of the Y-shaped diagram consists of two distinct branches, one of which is found to contain a far larger number of nebulae than in the other. The principal branch contains the normal “spiral” nebulae, which are characterized by a circular nucleus from which emerge two (or occasionally more) arms of approximately spiral shape. (...) These nebulae are subdivided into three classes, designated  $Sa, Sb, Sc$ , class  $Sa$  fitting almost continuously on to class  $E7$ .

The minor branch contains a special class of spirals characterized by the circumstance that the spiral arms appear to emerge from the

two ends of a straight bar-shaped or spindle-shaped mass. (...)

About 97 per cent of known extra-galactic nebulae are found to fit into this Y-shaped classification. The remaining 3 per cent, are of irregular shape, and refuse to fit into the classification at all. (...) The irregular nebulae are distinguished by a complete absence of symmetry of figure and also by the absence of any central nucleus. (...)

Apart from the irregular nebulae, Hubble states that, out of more than a thousand nebulae examined, less than a dozen refused to fit into the Y-shaped diagram at all, while in less than 10 per cent of the cases was there any considerable doubt as to a proper position of a nebula in the diagram. Clearly, the Y-shaped diagram provides a highly satisfactory working classification."

A more detailed description of the classification scheme was performed later (Hubble 1936), and subsequently modified as the collection of large-scale plates of giant galaxies grew. Reproductions of many of these plates were published posthumously (Sandage 1961) and the introduction therein is generally regarded as the definitive exposition of the Hubble scheme. At the junction of elliptical and spiral galaxies, comes a class of galaxies (not mentioned in early classifications) known as lenticulars. These galaxies are designated as type *S0* or type *SB0* according to whether or not they are barred. For further details refer to e.g., Mihalas & Binney (1981, Chap. 5, § 5.1).

The Hubble system, as conceived by Hubble and further developed by Sandage, is defined in terms of type-examples which are almost exclusively giant galaxies ( $M_{pg} \leq -19$ ). However, the most numerous type of galaxy in the Local Group is either dwarf elliptical or dwarf spheroidal. The surface brightness of a typical object belonging to the former class, is perfectly normal for an elliptical galaxy, so that it differs from a giant elliptical galaxy only in linear size and absolute magnitude. Dwarf spheroidal galaxies, on the other hand, are very low surface brightness objects. Thus it may safely be expected that dwarf galaxies are the most numerous objects in the universe.

Hubble's original scheme has generally been considered satisfactory in regard to the ellipticals, but it has been said that Hubble's classification of the spirals is incomplete and that his treatment of irregular galaxies was quite inadequate. A few of the more important attempts at reclassification

of types later than  $E$  (that is, to the right side of the ellipticals in Hubble's diagram) are described below.

Hubble's two-dimensional scheme has been made three-dimensional to include explicit reference to rings and s-shaped objects, and, in addition, the sequence has been extended to  $Sd$ - $m$  and  $Im$  galaxies (de Vaucouleurs 1959). The  $Sd$  class overlaps Hubble's  $Sc$  class to some extent, but it also contains more extreme objects which are classified as Type I Irregulars ( $Irr\ I$ ) in Hubble's scheme. The  $Sm$  and  $Im$  classes contain the remaining galaxies of Hubble's  $Irr\ I$  class.

An alternative scheme (the Yerkes system) relies on a fundamental parameter designating the population group or concentration class of a galaxy (McClure & van den Bergh 1968; Morgan et al. 1975). This parameter runs from  $k$  to  $a$  such that, among normal (in the sense of "non active") galaxies, those of type  $k$  have the highest degree of central concentration of their light, and those of type  $a$  have the smallest central bulges and the most diffuse light distributions. Galaxies of type  $gk$ ,  $g$ ,  $fg$ ,  $f$ ,  $af$ , have various intermediate light concentration.

Many features of both the classical Hubble system and the Yerkes system are incorporated in a new scheme (the DDO system), where the lenticular galaxies are arranged parallel to the spirals rather than before them, and a new class of galaxy, the "anemic" spiral, is interposed between the spirals and the lenticulars (van den Bergh 1960a,b; 1976). The resulting figure is a trident diagram, and the related sequences of barred galaxies are described by a separate trident.

For further details and references on the classical Hubble system, the de Vaucouleurs system, the Yerkes system, and the DDO system, see e.g., Mihalas & Binney (1981, Chap. 5, § 5.1). A deep analysis on the physical parameters along the Hubble sequence may be found in e.g., Roberts & Haynes (1994). The variation of gas content along the Hubble sequence may be explored using a new catalogue of normal (in the sense of "isolated") galaxies (Bettoni et al. 2003).

## 5.2 Physical interpretation

Soon after the early Hubble (1926) classification of the "great nebulae", a physical interpretation was provided by Jeans (1929, Chap. XIII, § 299):

Obviously the proper physical interpretation of the classification just described is of the utmost importance to cosmogony.

A first and most important clue is provided by the fact that numbers of the great nebulae are known to be in rotation. (...)

The symmetry of figure shewn by nebulae of the *E* and *Sa* types is precisely such as rotation might be expected to produce, and this suggests an inquiry as to how far the observed figures of the regular nebulae can be explained as the figures assumed by masses rotating under their own gravitation".

The conclusion is (Jeans 1929, Chap. XIII, § 302):

"Remembering that rotation has actually been observed in a number of nebulae, there seem to be strong reasons for conjecturing that the observed configuration of the nebulae may be explained in general terms as the configurations of rotating masses".

More specifically, two classes of models are considered, where density profiles range between the limiting cases (i) homogeneous configurations i.e. classical MacLaurin spheroids and Jacobi ellipsoids, and (ii) mass points surrounded by massless atmospheres i.e. Roche systems. Rigidly rotating mass distributions of the kind considered may attain any shape between the extreme boundaries (a) spherical i.e. nonrotating, and (b) centrifugal support at the end of major equatorial axis. With respect to the latter configuration, further rotation implies equatorial shedding or top major equatorial axis streaming of matter, for axisymmetric and triaxial configurations, respectively. For a fixed density profile, the sequence of rigidly rotating configurations starts from the spherical shape and ends at the shape where centrifugal support is first attained.

The above interpretation suffers from two main points (Jeans 1929, Chap. XIII, §§ 300-302). First, the most flattened elliptical configuration (if related to a figure of revolution), should occur when centrifugal support takes place at the bifurcation point, from axisymmetric to triaxial shapes. On the other hand, the above mentioned limiting configuration is less flattened than *E7*. Second, triaxial bodies of the kind considered cannot be figures of equilibrium if a great central condensation of mass is present. On the other hand, it is the case for barred spirals.

Owing to the results of Sect. 3, homeoidally striated Jacobi ellipsoids with arbitrary peculiar velocity field, and systematic motions reduced to rotation around a fixed axis, may be related to classical Jacobi ellipsoids, provided imaginary rotation is taken into consideration. Then the occurrence of anisotropic peculiar velocity distributions does not affect the physical interpretation under discussion, and the questions to be clarified remain the above mentioned two.

Accordingly, the second sentence quoted from Jeans at the beginning of the current Section, could be generalized as: “*A first and most important clue is provided by the fact that galaxies are known to be in (real or imaginary) rotation*”. In particular (i) spiral galaxies apparently rotate; (ii) faint ( $M_B > -20.5$ ) elliptical galaxies (Davies et al. 1983), *SA* bulges (Kormendy & Illingworth 1982), *SB* bulges (Kormendy 1982), and a few bright ( $M_B < -20.5$ ) elliptical galaxies (Illingworth 1981) appear to be supported by systematic rotation; (iii) the majority of bright elliptical galaxies (Illingworth 1981) appear to be supported by anisotropic peculiar velocity distribution; and (iv) elliptical-like galaxies with dust lanes (Sharples et al. 1983), similarly to bright ellipticals, appear to be supported by either systematic rotation or anisotropic peculiar velocity distribution. For a more detailed discussion refer to Caimmi (1983).

In absence of a unified theory of systematic and random motions, with regard to rotation around a fixed axis, centrifugal support and anisotropic pressure must necessarily be thought of as independent contributions to the shape of the system (e.g., Binney 1976, 1978, 1980). On the contrary, the current attempt comes back to Jean’s conception, that the shape of galaxies is determined by rotation, conceived as real (related to centrifugal support) or imaginary (related to anisotropic peculiar velocity distribution). To this aim, our attention shall be restricted to the Hubble classification for the following reasons. First, it is defined in terms of almost exclusively bright galaxies, where both centrifugal support and anisotropic peculiar velocity distribution have been observed. Second, it has generally been considered satisfactory in regard to ellipticals.

The detection of highly flattened ellipticals is expected to be rare, as they must necessarily be viewed edge-on. In addition, the advent of more refined instruments and techniques has led to different classifications. For instance, NGC 3115 is quoted as *E7* in Jeans (1929, Chap. XIII, §298, Plate IX), *E7/S0* in Sandage’s Hubble Atlas of Galaxies (e.g., Mihalas & Binney 1981,

Chap. 5, § 5.1, Fig. 5.3), and  $S0$  in Larsen et al. (1983); NGC 3377 is quoted as  $E6$  in Sandage’s Hubble Atlas of Galaxies (e.g., Mihalas & Binney 1981, Chap. 5, § 5.1, Fig. 5.3),  $E5\text{-}6$  in Copin et al. (2004); and the junction of the elliptical and spiral galaxies occurs at  $E7$  type in the Hubble’s fork diagram (e.g., Mihalas & Binney 1981, Chap. 5, § 5.1, Fig. 5.2) and at  $E6$  type in the van den Bergh’s trident diagram (e.g., Mihalas & Binney 1981, Chap. 5, § 5.1, Fig. 5.8). Additional examples of highly flattened ( $E6$ ) ellipticals are NGC 821 and NGC 4697 which, together with NGC 3377, are known to host supermassive ( $M \approx 10^8 M_\odot$ ) black holes (Soria et al. 2006). Different features exhibited by highly flattened elliptical and lenticular galaxies, are shown by typical objects belonging to each class, as in the cases shortly reported below.

NGC 3377 is a prototypical “disky” elliptical galaxy with “boxy” outer isophotes. It has a power-law central luminosity profile and its total absolute magnitude of about  $-19(B)$  is intermediate between that of the classical “boxy” giant ellipticals and “disky” lower-luminosity objects. Both dynamical model and the  $M_* - \sigma$  relation suggest the presence of a massive black hole. For further details and references refer to e.g., Copin et al. (2004); Soria et al. (2006).

NGC 3115 has long been assumed to be the prototype of the  $S0$  galaxy type: a bulge-dominated galaxy with an embedded disk and very little gas and dust. The system has a nearly edge-on inclination and contains a double disk structure with an outer Freeman type II disk, which exhibits a weak spiral arm structure, and a nuclear disk of size about fifty times shorter. The spheroidal component does not seem to follow the classical  $r^{1/4}$  law, and the flattened halo extends up to nine times outside the larger disk. The bulge appears to be supported by systematic rotation and evidence has been found for the presence of both a central dark mass and a massive dark halo. For further details and references refer to e.g., Emsellem et al. (1999).

### 5.3 The $E$ sequence within Ellipsoidland

In dealing with a physical interpretation of the early Hubble sequence, it is convenient to define axis ratios of intrinsic configurations in a different way. Given a homeoidally striated Jacobi ellipsoid, let  $a, b, c$ , be the semiaxes, where  $a \geq b \geq c$  without loss of generality. Accordingly,  $\epsilon_{ca} \leq \epsilon_{ba} \leq 1$ ; in addition, the minor and the major axis coincide with the rotation axis for oblate-like and prolate-like configurations, respectively.

The whole range of possible configurations in the  $(O\epsilon_{ba}\epsilon_{ca})$  plane defines Ellipsoidland (the term is from Hunter & de Zeeuw 1997). Ellipsoidland is a triangle where two sides are of unit length and an angle is right, as shown in Fig. 1. Oblate configurations lie on the vertical side,  $\epsilon_{ba} = 1$ , the spherical configuration (square) is on the top,  $\epsilon_{ca} = 1$ , and the flat circular configuration is on the bottom,  $\epsilon_{ca} = 0$ . Prolate configurations lie on the inclined side,  $\epsilon_{ca} = \epsilon_{ba}$ , the spherical configuration is on the top,  $\epsilon_{ca} = \epsilon_{ba} = 1$ , and the prolate oblong configuration is on the bottom,  $\epsilon_{ca} = \epsilon_{ba} = 0$ . Flat configurations lie on the horizontal side,  $\epsilon_{ca} = 0$ , the flat circular configuration is on the right,  $\epsilon_{ba} = 1$ , and the flat oblong configuration is on the left,  $\epsilon_{ba} = 0$ . It is worth noticing that flat-oblong and prolate-oblong configurations are not coincident (e.g., Caimmi 1993; CM05). Non flat, non axisymmetric configurations, lie within Ellipsoidland.

The axis ratio correlation,  $\epsilon_{ca}$  vs.  $\epsilon_{ba}$ , related to adjoint configurations to homeoidally striated Jacobi ellipsoids, is represented within Ellipsoidland in Fig. 1. The bifurcation point from MacLaurin spheroids to Jacobi ellipsoids is marked by a triangle. The bifurcation point from MacLaurin spheroids and Jacobi ellipsoids to pear-shaped configurations is marked by a St. Andrew's cross and a Greek cross, respectively. With regard to real rotation, the correlation is the known one involving classical MacLaurin spheroids and Jacobi ellipsoids. With regard to imaginary rotation, the correlation reads  $\epsilon_{ca} = \epsilon_{ba}$ , owing to lack of bifurcation points. Then configurations in real and imaginary rotation branch off from the nonrotating spherical configuration. The former sequence proceeds down along the oblate side of Ellipsoidland, until the bifurcation point is attained and the curve enters Ellipsoidland, finishing when the next bifurcation point is also attained. The latter sequence proceeds down along the prolate side of Ellipsoidland, until the prolate-oblong configuration is attained, never entering Ellipsoidland. On the other hand, a sequence may stop earlier, when centrifugal support at the ends of major equatorial axis is attained, which depends on the density profile. In fact, it makes the sole difference between homeoidally striated Jacobi ellipsoids and their adjoint counterparts (for further details, see CM05).

With regard to Ellipsoidland, the observed lack of elliptical galaxies more flattened than  $E7$  translates into the inequality,  $\epsilon_{ca} \geq 0.25$ , the threshold being represented by the lower dashed horizontal line in Fig. 1. The locus of edge-on configurations, viewed along a direction coinciding with equatorial minor axis, where  $0.25 \leq \epsilon_{ca} \leq 0.35$ , and then belonging to class  $E7$ , is

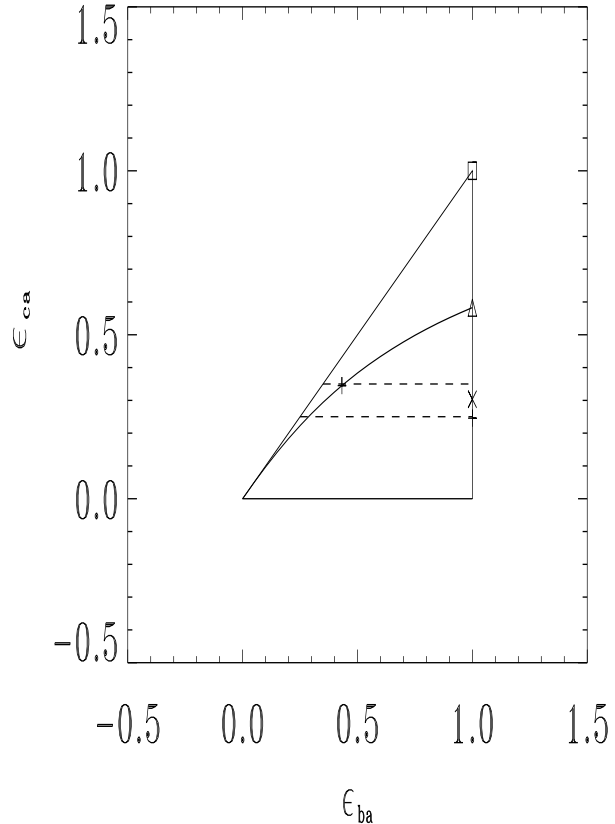


Figure 1: Axis ratio correlation within Ellipsoidland, with regard to adjoint configurations to homeoidally striated Jacobi ellipsoids. The semiaxes are  $a$ ,  $b$ ,  $c$ , where  $a \geq b \geq c$  or  $\epsilon_{ca} \leq \epsilon_{ba} \leq 1$ , without loss of generality. The locus of flat configurations is  $\epsilon_{ca} = 0$ ,  $0 \leq \epsilon_{ba} \leq 1$ . The locus of oblate configurations is  $\epsilon_{ba} = 1$ ,  $0 \leq \epsilon_{ca} \leq 1$ . The spherical configuration (square) is defined as  $\epsilon_{ca} = \epsilon_{ba} = 1$ . The oblong configuration is defined as  $\epsilon_{ca} = \epsilon_{ba} = 0$ . The locus of prolate configurations is  $\epsilon_{ca} = \epsilon_{ba}$ ,  $0 \leq \epsilon_{ba} \leq 1$ . Different configurations occur in the flat oblong limit,  $\epsilon_{ca} = 0$ ,  $\epsilon_{ba} \rightarrow 0$ , and in the prolate oblong limit,  $\epsilon_{ca} \rightarrow 0$ ,  $\epsilon_{ba} \rightarrow 0$ ,  $\epsilon_{ca} = \epsilon_{ba}$ . A band, bounded by two horizontal dashed lines, defines class  $E7$  in Hubble (1926) classification i.e.  $0.25 < \epsilon_{ca} \leq 0.35$  for edge-on ellipsoids where the line of sight coincides with the direction of the minor equatorial axis. The bifurcation point from MacLaurin spheroids to Jacobi ellipsoids is marked by a <sup>31</sup> triangle. The bifurcation point from MacLaurin spheroids and Jacobi ellipsoids to pear-shaped configurations is marked by a St. Andrew's cross and a Greek cross, respectively.

represented in Fig. 1 as a band bounded by two dashed lines,  $\epsilon_{ca} = 0.25$  and  $\epsilon_{ca} = 0.35$ , respectively. A change in direction of the line of sight could project an intrinsic ellipsoid within the above mentioned band, on a class  $Ei$ ,  $i < 7$ .

An inspection of Fig. 1 shows that the bifurcation points from triaxial and axisymmetric configurations, towards pear-shaped configurations, are consistent, or marginally consistent, with the  $E7$  band on Ellipsoidland. Then the occurrence of triaxiality provides a physical interpretation to the observed absence of elliptical galaxies (and spiral bulges) more flattened than  $E7$ , with regard to the oblate-like branch of the sequence. On the other hand, the above interpretation cannot apply to the prolate branch of the sequence, as no bifurcation point has been found therein, and some kind of instability must be considered.

The absence of elliptical galaxies more flattened or elongated than  $E7$  might be due to bending instabilities, as suggested long time ago from analytical considerations involving homogeneous (oblate and prolate) spheroids (Polyachenko & Shukhman 1979; Fridman & Polyachenko 1984, Vol. 1, Chap. 4, Sect. 3.3, see also pp. 313-322; Vol. 2, p. 159) and numerical simulations involving inhomogeneous (oblate and prolate) spheroids (Merritt & Hernquist 1991; Merritt & Sellwood 1994). The amount of figure rotation seems to be unimportant to this respect (Raha et al. 1991; Merritt & Sellwood 1994).

This conclusion is supported by recent results from  $N$ -body numerical simulations, where spherically symmetric, unstable, radially anisotropic, one-component  $\gamma$  models were taken as starting configurations (Nipoti et al. 2002). The related end-products, in accordance with previous results (e.g., Merritt & Aguilar 1985; Stiavelli & Sparke 1991), were found to be in general prolate systems less flattened than  $E7$  (Nipoti et al. 2002, Fig. 1 therein).

The theoretical explanation of the result, in terms of a dynamical bending instability (Merritt & Sellwood 1994), is generally recognized to explain also the maximum elongation of simulated nonbaryonic dark matter haloes (e.g., Bett et al. 2007).

## 5.4 Tidal effects from hosting dark matter haloes

Current  $\Lambda$ CDM cosmologies, which provide a satisfactory fit to data from primordial nucleosynthesis and cosmic background radiation, predict galaxies are embedded within dark matter haloes. Then it is a natural question

to what extent the presence of hosting dark matter haloes may affect the above interpretation of the early Hubble sequence. To this aim, an idealized situation shall be analysed.

Let us represent elliptical galaxies and their hosting dark haloes as concentric and coaxial classical Jacobi ellipsoids, one completely lying within the other. Accordingly, the two bodies must necessarily rotate at the same extent, and/or one of them (the outer in the case under discussion) has to be axisymmetric. It can be seen that the effect of the outer ellipsoid on the inner one is to shift bifurcation points towards more flattened configurations with respect to a massless embedding subsystem (Durisen 1978; Pacheco et al. 1986; Caimmi 1996a).

More specifically, the axis ratio of the configuration at the bifurcation point is the solution of the transcendental equation (Caimmi 1996a):

$$\frac{[(\epsilon_i)_{31}]^2 (A_i)_3}{(A_i)_1} = \left[ \frac{5 - 4[(\epsilon_i)_{31}]^2}{3 - 2[(\epsilon_i)_{31}]^2} + \kappa \frac{4 - 4[(\epsilon_i)_{31}]^2}{3 - 2[(\epsilon_i)_{31}]^2} \right]^{-1} ; \quad (86a)$$

$$m = \frac{M_j}{M_i} ; \quad y_k = \frac{(a_j)_k}{(a_i)_k} ; \quad \frac{m}{y_1 y_2 y_3} = \frac{\rho_j}{\rho_i} ; \quad (86b)$$

$$\kappa = \frac{m}{y_1 y_2 y_3} \frac{(A_j)_3}{(A_i)_3} ; \quad 0 \leq \kappa < +\infty ; \quad (86c)$$

where the indices,  $i, j$ , denote inner and outer ellipsoid, respectively. In the special case of massless outer ellipsoid,  $\kappa = 0$ , Eq. (86a) reduces to (75).

Further analysis shows that the embedded configuration, at the bifurcation point, can be as flattened as  $E7$  provided the parameter,  $\kappa$ , is close to unity. On the other hand, the related parameters are to be consistent with observations and cosmological models. To this aim, inhomogeneous density profiles must be considered.

The generalization of Eq. (86a) to homeoidally striated Jacobi ellipsoids demands to restart from a generalized formulation of the virial theorem, where the tidal potential is also included (Brosche et al. 1983; Caimmi et al. 1984; Caimmi & Secco 1992). The repetition of the same procedure used in the current paper, yields:

$$\kappa = \frac{m}{y_1 y_2 y_3} \frac{(\nu_{ij})_{\text{tid}}}{(\nu_i)_{\text{sel}}} \frac{(A_j)_3}{(A_i)_3} ; \quad (87)$$

where  $(\nu_{ij})_{\text{tid}}$  is an additional factor in the expression of the potential tidal energy, related to the tidal action of the embedding subsystem on the embedded one (Caimmi 2003; CM05).

It may safely be expected that the external boundary is less flattened than the internal one and more flattened than a sphere. Accordingly, the shape factor ratio appearing in Eqs. (87), ranges as  $1/2 < (A_j)_3/(A_i)_3 < 1$  for oblate configurations, and  $1 < (A_j)_3/(A_i)_3 < 10/3$  for prolate configurations. Then, to a first extent,  $(A_j)_3/(A_i)_3 \approx 1$ , i.e. the boundaries are similar and similarly placed ellipsoids. With this restriction, the factor,  $(\nu_{ij})_{\text{tid}}$ , is a profile factor, which may be expressed by a simple formula (Caimmi 2003):

$$(\nu_{ij})_{\text{tid}} = -\frac{9}{8} \frac{m\Xi_i}{(\nu_i)_{\text{mas}}(\nu_j)_{\text{mas}}} w^{(\text{ext})} \frac{\Xi_i}{y_0} ; \quad (88)$$

where  $y_0$  is the scaling radius ratio of outer to inner subsystem, and  $w^{(\text{ext})}$  is an additional profile factor.

Typical elliptical galaxies and their hosting dark haloes may safely be represented as homeoidally striated Jacobi ellipsoids, where the star and dark subsystem are described by generalized power-law density profiles of the kind:

$$f_u(\xi_u) = \frac{2^\chi}{\xi_u^\gamma (1 + \xi_u^\alpha)^\chi} ; \quad \chi = \frac{\beta - \gamma}{\alpha} ; \quad u = i, j ; \quad (89a)$$

$$\xi_u = \frac{r_u}{(r_0)_u} ; \quad \Xi_u = \frac{R_u}{(r_0)_u} ; \quad (89b)$$

$$\xi_i = y_0 \xi_j ; \quad y \Xi_i = y_0 \Xi_j ; \quad (89c)$$

$$y_0 = \frac{(r_0)_j}{(r_0)_i} ; \quad y = \frac{R_j}{R_i} ; \quad (89d)$$

according to Eqs. (1), and the choices  $(\alpha, \beta, \gamma) = (1, 4, 1)$  (Hernquist 1990) and  $(\alpha, \beta, \gamma) = (1, 3, 1)$  (Navarro et al. 1995, 1996, 1997) are adopted to describe the star and the dark subsystem, respectively. The values of input and output parameters of the model are listed in Tab. 1, with regard to a  $\Lambda$ CDM cosmology where  $\Omega_M = 0.3$ ,  $\Omega_\Lambda = 0.7$ ,  $\Omega_b = 0.0125h^{-2}$ ,  $h = 2^{-1/2}$ . For further details and references, see CM03, CM05.

The presence of a massive halo has little influence on the location of the bifurcation point from axisymmetric to triaxial configurations, which is found to occur at an axis ratio,  $(\epsilon_{31})_{\text{bif}} = 0.580088$ , related to  $\kappa = 0.00441624$ .

input	value	output	value
$\Xi_i$	$40/3$	$(\nu_i)_{\text{mas}}$	10.38399
$\Xi_j$	10	$(\nu_j)_{\text{mas}}$	17.86565
$(r_0)_i/\text{kpc}$	3.21	$(\nu_i)_{\text{sel}}$	1.44444
$(r_0)_j/\text{kpc}$	36.20	$(\nu_j)_{\text{sel}}$	0.6268271
$R_i/\text{kpc}$	42.77	$(\nu_{ij})_{\text{tid}}$	0.3518317
$R_j/\text{kpc}$	362.04	$(\nu_{ji})_{\text{tid}}$	0.2217760
$M_i/10^{10} M_\odot$	8.33	$(\nu_i)_{\text{rot}}$	$1/3$
$M_j/10^{10} M_\odot$	91.67	$(\nu_j)_{\text{rot}}$	$1/3$
$y_0$	11.29	$(\eta_i)_{\text{rot}}$	$1/2$
$y$	8.47	$(\eta_j)_{\text{rot}}$	$1/2$
$m$	11	$w^{(\text{est})}$	-0.3955800
		$w^{(\text{int})}$	-3.564028
		$(\nu_{ij})_{\text{int}}$	1.760852
		$(\nu_{ji})_{\text{int}}$	1.760852
		$\left(\frac{2\eta_{\text{rot}}\nu_{\text{rot}}}{\nu_{\text{sel}}}\right)_i$	0.230769
		$\left(\frac{2\eta_{\text{rot}}\nu_{\text{rot}}}{\nu_{\text{sel}}}\right)_j$	0.531779
		$\frac{m}{y^3} \frac{(\nu_{ij})_{\text{tid}}}{(\nu_i)_{\text{sel}}}$	0.00441624
		$(\epsilon_{31})_{\text{bif}}$	0.580088

Table 1: Values of input and output parameters in modelling elliptical galaxies and their hosting dark haloes as similar and similarly placed, homeoidally striated Jacobi ellipsoids, characterized by Hernquist (1990) and Navarro et al. (1995, 1996, 1997) density profiles, respectively. The parameters of the related  $\Lambda$ CDM cosmology have been chosen as  $\Omega_M = 0.3$ ,  $\Omega_\Lambda = 0.7$ ,  $\Omega_b = 0.0125h^{-2}$ ,  $h = 2^{-1/2}$ . For further details on the output parameters see e.g., CM03.

A similar result is expected to occur for the bifurcation point from both axisymmetric and triaxial to pear-shaped configurations. Then the above mentioned points continue to be consistent, or marginally consistent, with the  $E7$  band on Ellipsoidland, even in presence of (typical) massive dark haloes, concerning the oblate-like branch of the sequence. On the contrary, it is suggested the existence of some kind of instability, which does not allow prolate configurations in rigid imaginary rotation, more elongated than  $E7$ , even in presence of (typical) massive dark haloes, according to recent results from  $N$ -body simulations (Nipoti et al. 2002).

## 5.5 Cosmological effects after decoupling

About thirty years ago, Thuan & Gott (1975) idealized elliptical galaxies as MacLaurin spheroids, resulting from virialization after cosmological expansion and subsequent collapse and relaxation of their parent density perturbation. A generalization of the method to triaxial configurations and anisotropic peculiar velocity distributions, has been performed in CM05, and an interested reader is addressed therein for further details. Owing to the results of Sect. 3, the case of isotropic peculiar velocity distribution, involving both real and imaginary rotation, can be considered without loss of generality.

Our attention shall be limited to dark matter haloes hosting giant galaxies, as massive as about  $10^{12} M_\odot$ . Accordingly, it is assumed  $\bar{\delta}_{rec} = 0.015$  as a typical overdensity index of the initial configuration, taken to be at recombination epoch, and a relaxed final configuration i.e.  $\zeta = 1$ .

With regard to the initial configuration, the following approximations hold to a good extent: (i) spherical shape; (ii) homogeneous mass distribution; (iii) negligible rotation energy; (iv) negligible peculiar energy. The changes in mass, angular momentum, and total energy, respectively, during the transition from the initial to final configuration, are expressed by the parameters,  $\beta_M$ ,  $\beta_J$ ,  $\beta_E$ , defined by Eqs. (78b) and (79b), where the initial configuration is marked by the prime. For further details, see CM05.

Though negligible with respect to the potential and expansion energy, the rotation energy of the initial configuration affects the shape of the final configuration, as described by Eqs. (78), (81), (83), (85), where different changes in mass, angular momentum, and tidal energy, are related to a same final shape for an assigned initial configuration, provided the parameter,  $\beta_\varepsilon$ ,

defined by Eq. (85), does not vary. The choice,  $\beta_{\mathcal{E}} = 1/3600$ , in particular  $(\beta_M, \beta_J, \beta_E) = (1, 60, 1)$ , holds for dark matter haloes hosting giant elliptical galaxies, and it shall be assumed here. For further details, see CM05.

The axis ratios of the final configuration,  $\epsilon_{31}$  and  $\epsilon_{21}$ , as a function of the parameter,  $\kappa_{\mathcal{E}} = \mathcal{E}'_{\text{rot}}/(1 - \mathcal{E}'_{\text{osc}} - \mathcal{E}'_{\text{pec}})$ , are plotted in Fig. 2, with regard to a Navarro et al. (1995, 1996, 1997) density profile ( $\Xi = 9.20678$ ; see CM05, Tab. 1 therein, for further details) in rigid rotation. Each curve is symmetric with regard to a vertical axis,  $\kappa_{\mathcal{E}} = 0.5$ , where a local minimum is attained. The plane,  $(\mathcal{O}\kappa_{\mathcal{E}}\epsilon)$ , may be divided into three regions, namely (a)  $0.163190 \leq \kappa_{\mathcal{E}} \leq 0.836810$ , where triaxial configurations occur, ranging from  $(\epsilon_{21}, \epsilon_{31}) = (1, 0.582724)$  to  $(\epsilon_{21}, \epsilon_{31}) = (0.363174, 0.302297)$ , the latter related to  $\kappa_{\mathcal{E}} = 0.5$ ; (b)  $0 \leq \kappa_{\mathcal{E}} \leq 0.163190$ ,  $0.836810 \leq \kappa_{\mathcal{E}} \leq 1$ , where oblate configurations occur, ranging from  $(\epsilon_{21}, \epsilon_{31}) = (1, 0.582724)$  to  $(\epsilon_{21}, \epsilon_{31}) = (1, 1)$ , the latter related to  $\kappa_{\mathcal{E}} = 0$  (bound),  $\kappa_{\mathcal{E}} = 1$  (unbound), respectively; (c)  $-\infty < \kappa_{\mathcal{E}} \leq 0$ ,  $1 \leq \kappa_{\mathcal{E}} < +\infty$ , where prolate configurations occur, ranging from  $(\epsilon_{21}, \epsilon_{31}) = (1, 1)$  to  $(\epsilon_{21}, \epsilon_{31}) = (1, +\infty)$ , the latter related to  $\kappa_{\mathcal{E}} \rightarrow -\infty$  (bound),  $\kappa_{\mathcal{E}} \rightarrow +\infty$  (unbound), respectively. It is worth recalling that oblate-like ( $\epsilon_{31} \leq \epsilon_{21} \leq 1$ ) and prolate-like ( $\epsilon_{21} \leq 1 \leq \epsilon_{31}$ ) configurations, are related to real and imaginary rotation, respectively.

An inspection of Fig. 2 shows that, in the case under discussion, cosmological effects due to expansion prevent dark matter haloes in real rotation from being more flattened than  $E7$  (dashed horizontal band). The same holds for embedded giant elliptical galaxies, provided the related shapes may safely be thought of as similar and similarly placed. On the other hand, an arbitrary flattening can be attained by dark matter haloes in imaginary rotation, unless some kind of instability occurs, which similarly prevents configurations more elongated than  $E7$ .

As outlined in Subsect. 5.3, bending instabilities have been suggested long time ago as a viable mechanism to this respect (Polyachenko & Shukhman 1979; Fridman & Polyachenko 1984, Vol. 1, Chap. 4, Sect. 3.3, see also pp. 313–322; Vol. 2, p. 159; Merritt & Hernquist 1991; Merritt & Sellwood 1994).

The above results depend on both density profile and rotation velocity profile of the final configuration, via the coefficient,  $c$ , appearing in Eq. (81c). Owing to Eqs. (7) and (18c), Eq. (81c) translates into:

$$c = \beta_{\mathcal{E}'} \frac{\mathcal{R}'}{(\mathcal{S}')^2} \frac{(B_{\text{sel}})^2}{B_{\text{ram}}} \mathcal{E}_{\text{rot}} \left[ \frac{2\zeta - 1}{2\zeta} - \frac{\zeta - 1}{\zeta} \mathcal{E}_{\text{rot}} \right] ; \quad (90a)$$

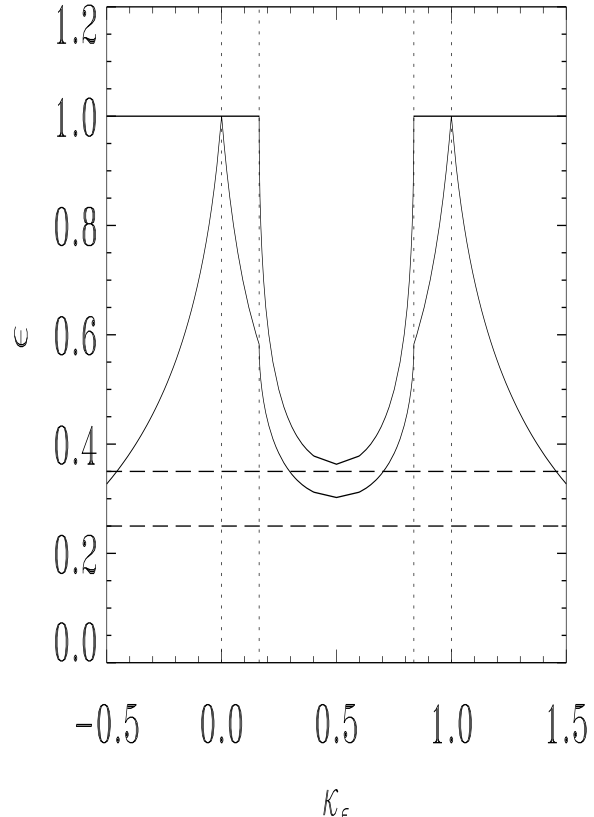


Figure 2: Equatorial (upper curve) and meridional (lower curve) axis ratio of the final configuration, as a function of the parameter,  $\kappa_{\mathcal{E}} = \mathcal{E}'_{\text{rot}}/(1 - \mathcal{E}'_{\text{osc}} - \mathcal{E}'_{\text{pec}})$ , for sequences of relaxed Navarro et al. (1995, 1996, 1997) density profiles in rigid rotation, related to dark matter haloes hosting giant elliptical galaxies. The curves are symmetric with respect to a vertical axis,  $\kappa_{\mathcal{E}} = 0.5$ , and a minimum extremum point occurs at  $(\kappa_{\mathcal{E}}, \epsilon_{21}, \epsilon_{31}) = (0.5, 0.363174, 0.302297)$ , corresponding to the most flattened, oblate-like configuration which is allowed. Values of  $\kappa_{\mathcal{E}}$  within or outside the range,  $0 \leq \kappa_{\mathcal{E}} \leq 1$ , are related to real or imaginary rotation, respectively. Values of  $\kappa_{\mathcal{E}}$  below or not below unity, are related to bound (finite extent) and unbound (infinite extent) configurations, respectively. Oblate-like ( $\epsilon_{31} \leq \epsilon_{21} \leq 1$ ) triaxial configurations lie between the inner, vertical dotted lines. Oblate ( $\epsilon_{31} \leq \epsilon_{21} = 1$ ) axisymmetric configurations lie between the inner and the corresponding outer, vertical dotted lines. Prolate ( $\epsilon_{21} = 1 \leq \epsilon_{31}$ ) axisymmetric configurations lie outside the outer, vertical dotted lines. The equatorial axis ratio is  $\epsilon = \epsilon_{21}$ . The polar axis ratio is  $\epsilon = \epsilon_{31}$  for oblate and  $\epsilon = \epsilon_{13}$  for prolate configurations. The horizontal dashed lines define class *E7* in Hubble (1926) classification i.e.  $0.25 < \epsilon \leq 0.35$  for edge-on ellipsoids where the line of sight coincides with the direction of the minor equatorial

$$\beta_{\mathcal{E}'} = \beta_{\mathcal{E}} \frac{\nu_{\text{sel}}^2}{\nu_{\text{ram}}} = \frac{\beta_M^5}{\beta_J^2 \beta_E} \frac{\nu_{\text{sel}}^2}{\nu_{\text{ram}}} ; \quad (90b)$$

where different changes in mass, angular momentum, total energy, density profile, and rotation velocity profile, are related to the same final shape for an assigned final configuration, provided  $\beta_{\mathcal{E}'}$  does not vary. The choice,  $\beta_{\mathcal{E}'} = 6.007519 \cdot 10^{-6}$ , in particular  $(\beta_M, \beta_J, \beta_E, \nu_{\text{sel}}, \nu_{\text{ram}}) = (1, 60, 1, 0.610045, 17.20783)$ , holds for Fig. 2.

## 6 Conclusion

Elliptical galaxies have been modelled as homeoidally striated Jacobi ellipsoids where the peculiar velocity distribution is anisotropic, or equivalently as their adjoint configurations i.e. classical Jacobi ellipsoids of equal mass and axes, in real or imaginary rotation. Reasons for the coincidence of bifurcation points from axisymmetric to triaxial configurations in both the sequences (CM06), contrary to earlier findings (Wiegandt, 1982a,b; CM05), have been presented and discussed. The occurrence of centrifugal support at the ends of major equatorial axis, has been outlined.

The existence of a lower limit to the flattening of elliptical galaxies has been investigated in dealing with a number of limiting situations. More specifically, (i) elliptical galaxies have been considered as isolated systems, and an allowed region within Ellipsoidland (Hunter & de Zeeuw 1997), related to the occurrence of bifurcation points from ellipsoidal to pear-shaped configurations, has been shown to be consistent with observations; (ii) elliptical galaxies have been considered as embedded within dark matter haloes and, under reasonable assumptions, it has been shown that tidal effects from hosting haloes have little influence on the above mentioned results; (iii) dark matter haloes and embedded elliptical galaxies, idealized as a single homeoidally striated Jacobi ellipsoid, have been considered in connection with the cosmological transition from expansion to relaxation, by generalizing an earlier model (Thuan & Gott 1975), and the existence of a lower limit to the flattening of relaxed (oblate-like) configurations, has been established. On the other hand, no lower limit has been found to the elongation of relaxed (prolate-like) configurations, and the observed lack of elliptical galaxies more elongated than  $E7$  has needed a different physical interpretation such as the

occurrence of bending instabilities (Polyachenko & Shukhman 1979; Merritt & Hernquist 1991).

## 7 Acknowledgements

We are grateful to an anonymous referee for useful comments and remarks which improved an earlier version of the current paper. We are also indebted to D. Merritt and V. Polyachenko for pointing our attention to their (and coauthors') papers on bending instabilities, which had been overlooked in an earlier version of the current paper.

## References

- [1] Bertola, F., Capaccioli, M. 1975, *ApJ* 200, 439
- [2] Bertola, F., Galletta, G. 1978, *ApJ* 226, L115
- [3] Bett, P., et al. 2007, *MNRAS* 376, 215
- [4] Bettoni, D., Galletta, G., García-Burillo, S. 2003, *A&A* 405, 5
- [5] Binney, J. 1976, *MNRAS* 177, 19
- [6] Binney, J. 1978, *MNRAS* 183, 501
- [7] Binney, J. 1980, *MNRAS* 190, 421
- [8] Binney, J., & Tremaine, S. 1987, *Galactic Dynamics*, Princeton University Press, Princeton
- [9] Blaauw, A. 1965, in *Stars and Stellar Systems*, vol. V, Chap. 20, §3
- [10] Brosche, P., Caimmi, R., & Secco, L. 1983, *A&A* 125, 338
- [11] Caimmi, R. 1979, *ApSS* 71, 75
- [12] Caimmi, R. 1983, *ApSS* 93, 403
- [13] Caimmi, R., 1991, *ApSS* 180, 211

- [14] Caimmi, R. 1993a, ApJ 419, 615
- [15] Caimmi, R. 1993b, ApSS 199, 11
- [16] Caimmi, R., 1995, ApJ 441, 533
- [17] Caimmi, R. 1996a, Acta Cosmologica XXII, 21
- [18] Caimmi, R. 1996b, AN 317, 401
- [19] Caimmi, R. 2003, AN 324, 250
- [20] Caimmi, R. 2006, AN in press (C06)
- [21] Caimmi, R., Secco, L., Brosche, P. 1984, A&A 139, 411
- [22] Caimmi, R., Secco, L. 1992, ApJ 395, 119
- [23] Caimmi, R., & Marmo, C. 2003, NewA 8, 119 (CM03)
- [24] Caimmi, R., & Marmo, C. 2005, AN 326, 465 (CM05)
- [25] Chandrasekhar, S., Lebovitz, N.R. 1962, ApJ 136, 1082
- [26] Chandrasekhar, S. 1969, *Ellipsoidal Figures of Equilibrium*, Yale University Press, New Haven
- [27] Copin, Y., Cretton, N., Emsellem, E. 2004, A&A 415, 889
- [28] Davies, R.L., Efstathiou, G., Fall, S.M., Illingworth, G., Schechter, P.L. 1983, ApJ 266, 41
- [29] de Vaucouleurs, G. 1959, in *Handbuch der Physik*, vol. 53, Astrophysics IV: Stellar Systems, S. Flügge (ed.), Berlin, Springer-Verlag, p.275
- [30] Durisen, R.H. 1978, ApJ 224, 826
- [31] Emsellem, E., Dejonghe, H., Bacon, R. 1999, MNRAS 303, 495
- [32] Fridman, A., Polyachenko, V.L. 1984, *Physics of Gravitating Systems*, Springer-Verlag
- [33] Hernquist, L. 1990, ApJ 356, 359

- [34] Hoeft, M., Mücket, J.P., Gottlöber, S. 2004, ApJ 602, 162
- [35] Hubble, E.P. 1926, ApJ 64, 321
- [36] Hubble, E.P. 1936, *The Realm of Nebulae*, Yale University Press, New Haven
- [37] Hunter, C., & de Zeeuw, T.Z. 1997, ApJ 389, 79
- [38] Illingworth, G. 1977, ApJ 218, L43
- [39] Illingworth, G. 1981, in S. M. Fall and D. Lynden-Bell (eds.), *Structure and Evolution of Normal Galaxies*, Cambridge University Press, p. 27
- [40] Jeans, J. 1929, *Astronomy and Cosmogony*, Dover Publications, New York, 1961
- [41] Kormendy, J. 1982, ApJ 257, 75
- [42] Kormendy, J., Illingworth, G. 1982, ApJ 256, 460
- [43] Lai, D., Rasio, F.A., & Shapiro, S.L. 1993, ApJS 88, 205
- [44] Larsen, N., Norgaard-Nielsen, H.U., Kjærgaard, P., Dickens, R.J. 1983, A&A 117, 257
- [45] McClure, R.D., van den Bergh, S. 1968, AJ 73, 313
- [46] MacMillan, W.D. 1930, *The Theory of the Potential*, Dover Publications, New York, 1958
- [47] Marochnik, L.S. 1967, Soviet Astron. AJ 10, 738
- [48] Merritt, D., Aguilar, L.A. 1985, MNRAS 217, 787
- [49] Merritt, D., Hernquist, L. 1991, ApJ 376, 439
- [50] Merritt, D., Sellwood, J. 1994, ApJ 425, 551
- [51] Mihalas, D., Binney, J. 1981, *Galactic Astronomy*, W.H. Freeman and Company, S. Francisco
- [52] Morgan, W.W., Kayser, S., White, R.A. 1975, ApJ 199, 545

- [53] Navarro, J.F., Frenk, C.S., & White, S.D.M. 1995, MNRAS 275, 720
- [54] Navarro, J.F., Frenk, C.S., & White, S.D.M. 1996, ApJ 462, 563
- [55] Navarro, J.F., Frenk, C.S., & White, S.D.M. 1997, ApJ 490, 493
- [56] Nipoti, C., Londrillo, P., & Ciotti, L. 2002, MNRAS 332, 901
- [57] Pacheco, F., Pucacco, G., & Ruffini, R. 1986, A&A 161, 39
- [58] Pacheco, F., Pucacco, G., Ruffini, R., & Sebastiani, G. 1989, A&A 210, 42
- [59] Perek, L. 1962, Adv. Astron. Astrophys. 1, 165
- [60] Polyachenko, V.L., Shukhman, I.G. 1979, Sov. Astr. 27, 407
- [61] Raha, N., et al. 1991, Nature 352, 411
- [62] Rasia, E., Tormen, G., Moscardini, L. 2004, MNRAS 351, 237
- [63] Roberts, P.H. 1962, ApJ 136, 1108
- [64] Roberts, M.S., Haynes, M.P. 1994, ARAA 32, 115
- [65] Sandage, A. 1961, *The Hubble Atlas of Galaxies*, Carnegie Institution, Washington
- [66] Schechter, P.L., Gunn, J.E. 1979, ApJ 229, 472
- [67] Sharples, R.M., Carter, D., Hawarden, T.G., Langmore, A.J. 1983, MNRAS 202, 37
- [68] Soria, R., Graham, A.W., Fabbiano, G., Baldi, A., Elvis, M., Jerien, H., Pellegrini, S., Siemiginowska, A. 2006, ApJ 640, 143
- [69] Stiavelli, M., Sparke, L.S. 1991, ApJ 382, 466
- [70] Thuan, T.X., & Gott, J.R., III, 1975, Nature 257, 774
- [71] van den Bergh, S. 1960a, ApJ 131, 215
- [72] van den Bergh, S. 1960b, ApJ 131, 558

- [73] van den Bergh, S. 1976, ApJ 206, 883
- [74] Vandervoort, P.O., 1980a, ApJ 240, 478
- [75] Vandervoort, P.O., 1980b, ApJ 241, 316
- [76] Vandervoort, P.O., Welty, D.E. 1981, ApJ 248, 504
- [77] Wiegandt, R., 1982a, A&A 105, 326
- [78] Wiegandt, R., 1982b, A&A 106, 240

## Appendix

### A Some properties of ellipsoid shape factors

Ellipsoid shape factors,  $A_1$ ,  $A_2$ ,  $A_3$ , obey the following inequalities (Caimmi 1996a):

$$a_1^n A_1 \geq a_2^n A_2 \geq a_3^n A_3 ; \quad a_1 \geq a_2 \geq a_3 ; \quad n \geq 2 ; \quad (91a)$$

$$a_1^n A_1 \leq a_2^n A_2 \leq a_3^n A_3 ; \quad a_1 \geq a_2 \geq a_3 ; \quad n \leq 1 ; \quad (91b)$$

where inequalities (91a) and (91b), the latter restricted to  $n \leq 0$ , come from analytical considerations involving the explicit expression of the shape factors (e.g., MacMillan 1930, Chap.II, § 33;  $A_1 = \alpha^{-2}$ ,  $A_2 = \beta^{-2}$ ,  $A_3 = \gamma^{-2}$ , therein), and inequality (91b), restricted to  $0 < n \leq 1$ , results from an obvious generalization of a proof by Pacheco et al. (1989).

Using Eqs. (6) and (7) yields:

$$\frac{\mathcal{S}_{qq}}{\mathcal{S}_{33}} = \frac{A_q}{\epsilon_{3q}^2 A_3} ; \quad q = 1, 2 ; \quad (92)$$

and, owing to inequality (91a):

$$A_q \geq \epsilon_{3q}^2 A_3 ; \quad a_q \geq a_3 ; \quad q = 1, 2 ; \quad (93)$$

which implies  $\mathcal{S}_{qq} \geq \mathcal{S}_{33}$  for oblate-like configurations ( $a_q \geq a_3$ ), and  $\mathcal{S}_{qq} \leq \mathcal{S}_{33}$  for prolate-like configurations ( $a_q \leq a_3$ ).

In the limit of axisymmetric configurations,  $\epsilon_{21} = 1$ ,  $\epsilon_{31} = \epsilon$ ,  $A_1 = A_2 = \alpha$ ,  $A_3 = \gamma$ , and the following relations hold (e.g., Caimmi 1991, 1993):

$$\lim_{\epsilon \rightarrow 0} \alpha = 0 \quad ; \quad \lim_{\epsilon \rightarrow 0} \gamma = 2 \quad ; \quad \lim_{\epsilon \rightarrow 0} \frac{\alpha}{\epsilon} = \frac{\pi}{2} \quad ; \quad (94)$$

$$\lim_{\epsilon \rightarrow +\infty} \alpha = 1 \quad ; \quad \lim_{\epsilon \rightarrow +\infty} \gamma = \lim_{\epsilon \rightarrow +\infty} (\epsilon \gamma) = 0 \quad ; \quad \lim_{\epsilon \rightarrow +\infty} (\epsilon^2 \gamma) = +\infty \quad ; \quad (95)$$

$$\lim_{\epsilon \rightarrow 1} \frac{\gamma - \alpha}{1 - \epsilon^2} = \frac{2}{5} \quad ; \quad (96)$$

$$\frac{d\alpha}{d\epsilon} = \frac{1}{1 - \epsilon^2} \left[ (1 + 2\epsilon^2) \frac{\alpha}{\epsilon} - 2\epsilon \right] \quad ; \quad (97)$$

$$\frac{d\gamma}{d\epsilon} = \frac{1}{1 - \epsilon^2} \left[ (1 + 2\epsilon^2) \frac{\gamma}{\epsilon} - \frac{2}{\epsilon} \right] \quad ; \quad (98)$$

$$v = (v_N)_{\text{iso}} = \alpha - \epsilon^2 \gamma \quad ; \quad (99)$$

and keeping in mind the general property (e.g., Chandrasekhar 1969, Chap. 3, § 17):

$$A_1 + A_2 + A_3 = 2 \quad ; \quad (100)$$

it can be seen that the first derivative of the rotation parameter,  $dv/d\epsilon$ , is null provided the transcendental equation:

$$\alpha = \frac{6\epsilon^2}{1 + 8\epsilon^2} \quad ; \quad (101)$$

is satisfied. One solution is found to exist, which is related to oblate configurations. It corresponds to an extremum point where the function attains its maximum value (e.g., Chandrasekhar 1969, Chap. 5, § 32).

## B Wiegandt criterion for bifurcation

Given a collisionless, self-gravitating fluid in rigid rotation, where no internal energy transport occurs and the residual velocity is constant on the boundary, an upper limit for the point of bifurcation is (Wiegandt 1982a,b):

$$\Omega^2 I_{11} = V_{12;12} \quad ; \quad (102)$$

where  $V_{pq;rs}$  is the “super-matrix”:

$$V_{pq;rs} = \int_S \rho(x_1, x_2, x_3) x_p \frac{\partial \mathcal{V}_{rs}}{\partial x_q} d^3S \quad ; \quad (103)$$

$$\mathcal{V}_{rs}(x_1, x_2, x_3) = G \int_S \frac{\rho(x'_1, x'_2, x'_3)(x_p - x'_p)(x_s - x'_s)}{[(x_1 - x'_1)^2 + (x_2 - x'_2)^2 + (x_3 - x'_3)^2]^{3/2}} d^3S \quad (104)$$

which is expressed in terms of a generalized potential,  $\mathcal{V}_{rs}$ , and the integrations are carried over the whole volume,  $S$ , of the system.

In the special case of homeoidally striated Jacobi ellipsoids, Eq. (102) identifies the exact point of bifurcation (Wiegandt 1982a,b) and the following relations hold (Wiegandt 1982b):

$$V_{pq;pq} = -\frac{A_p - a_q^2 A_{pq}}{A_p} (E_{\text{sel}})_{pp} \quad ; \quad (105)$$

$$a_q^2 A_{pq} = \frac{A_p - A_q}{1 - \epsilon_{pq}^2} \quad ; \quad (106)$$

where the products,  $a_q^2 A_{pq}$ , are shape factors which depend on the axis ratios only, similarly to  $A_p$ , and symmetry with respect to the indices holds,  $A_{pq} = A_{qp}$ . In addition, Eq. (106) has been deduced from Chandrasekhar (1969, Chap. 3, § 21), Eq. (107) therein.

Though Wiegandt (1982b) analysis is restricted to binomial density profiles (e.g., Perek 1962; Chandrasekhar 1969, Chap. 3, § 20; Caimmi 1993), still it may be generalized to any kind of cored density profiles, defined as:

$$\rho_W(\xi) = \rho_c f(\xi_W) \quad ; \quad f(0) = 1 \quad ; \quad \rho_c = \rho(0) \quad ; \quad (107a)$$

$$\xi_W = \frac{r}{R} \quad ; \quad 0 \leq \xi_W \leq 1 \quad ; \quad \Xi_W = 1 \quad ; \quad (107b)$$

where the scaling radius and the scaling density are chosen to be equal to the radius,  $R$ , and the central density,  $\rho_c$ , respectively. The following relations:

$$\rho = \frac{\rho_0}{\rho_c} \rho_W \quad ; \quad \xi = \Xi \xi_W \quad ; \quad (108)$$

allow conversion from Eqs. (1) to Eqs. (107) and vice versa.

Using Eqs. (107), the mass, the inertia tensor, and the potential-energy tensor, take the equivalent expression:

$$M = (\nu_{\text{mas}})_W M_c \quad ; \quad (109a)$$

$$M_c = \frac{4\pi}{3} \rho_c a_1^3 \epsilon_{21} \epsilon_{31} \quad ; \quad (109b)$$

$$I_{pq} = \delta_{pq} \epsilon_{p1} \epsilon_{q1} a_1^2 M (\nu_{\text{inr}})_W ; \quad (110)$$

$$(E_{\text{sel}})_{pq} = -(\nu_{\text{sel}})_W \frac{GM^2}{a_1} (B_{\text{sel}})_{pq} ; \quad (111)$$

and the comparison with Eqs. (2), (3), (4), (8), yields:

$$(\nu_{\text{mas}})_W = \frac{\rho_0}{\rho_c} \frac{1}{\Xi^3} \nu_{\text{mas}} ; \quad (\nu_{\text{inr}})_W = \nu_{\text{inr}} ; \quad (\nu_{\text{sel}})_W = \nu_{\text{sel}} ; \quad (112)$$

finally, using Eqs. (6) and (109)-(112), the potential-energy tensor takes the equivalent form:

$$(E_{\text{sel}})_{pq} = -k\pi G \rho_c I_{pq} A_p ; \quad (113a)$$

$$k = \frac{4}{3} \frac{\rho_0}{\rho_c} \frac{\nu_{\text{sel}} \nu_{\text{mas}}}{\Xi^3 \nu_{\text{inr}}} ; \quad (113b)$$

being  $k$ , by definition, a profile factor.

Owing to Eqs. (8), (19), (21), (31), (32), (113b), the normalized rotation parameter, defined by Eq. (45), may be expressed as:

$$v_N = \frac{\Omega^2}{k\pi G \rho_c} ; \quad (114)$$

which coincides with the parameter,  $\phi$ , defined in Wiegandt (1982b) in the special case of rigid rotation ( $\nu_{\text{inr}} = \nu_{\text{rot}}$ ;  $\eta_{\text{rot}} = 1/2$ ; see CM05), as shown in Caimmi (1996b). Accordingly, Eq. (46) coincides with its Wiegandt (1982b) counterpart, Eq. (52) therein.

The combination of Eqs. (102), (105), (113), (114), yields:

$$v_N = A_1 - a_2^2 A_{12} ; \quad (115)$$

and the comparison with Eq. (46) reads:

$$a_2^2 A_{12} = \frac{\zeta_{11}}{\zeta_{33}} \epsilon_{31}^2 A_3 ; \quad (116)$$

in the limit of axisymmetric configurations,  $a_2 \rightarrow a_1$ ,  $A_{12} \rightarrow A_{11}$ , the left-hand side of Eq. (116) takes the expression (e.g., Caimmi 1995):

$$\lim_{a_2 \rightarrow a_1} a_2^2 A_{12} = \frac{1}{4} \left( 3A_1 - \epsilon_{31}^2 \frac{A_3 - A_1}{1 - \epsilon_{31}^2} \right) ; \quad (117)$$

and the combination of Eqs. (116), (117), yields:

$$\frac{\epsilon_{31}^2 A_3}{A_1} = \left[ \frac{5 - 4\epsilon_{31}^2}{3 - 2\epsilon_{31}^2} + \frac{4(1 - \epsilon_{31}^2)}{3 - 2\epsilon_{31}^2} \frac{\zeta_{11} - \zeta_{33}}{\zeta_{33}} \right]^{-1} ; \quad \epsilon_{21} = 1 ; \quad (118)$$

which is an explicit expression of Wiegandt (1982a,b) criterion for bifurcation, with regard to homeoidally striated Jacobi ellipsoids in rigid rotation. In the limit of isotropical residual velocity distribution,  $\zeta_{11} = \zeta_{22} = \zeta_{33}$ , Eq. (118) reduces to (Caimmi 1996a):

$$\frac{\epsilon_{31}^2 A_3}{A_1} = \frac{3 - 2\epsilon_{31}^2}{5 - 4\epsilon_{31}^2} ; \quad \epsilon_{21} = 1 ; \quad (119)$$

as expected.

The condition, defined by Eq. (118), has to be compared with its counterpart deduced in the current paper, under the same assumption i.e.  $\zeta_{11} = \zeta_{22}$  also for triaxial configurations. The latter may be deduced from Eq. (77), using the relation (e.g., Caimmi 1966a):

$$\lim_{\epsilon_{21} \rightarrow 1} \epsilon_{21}^2 \frac{A_2 - A_1}{1 - \epsilon_{21}^2} = \frac{1}{4} \left( 3A_1 - \epsilon_{31}^2 \frac{A_3 - A_1}{1 - \epsilon_{31}^2} \right) ; \quad (120)$$

and the result is again Eq. (118). Then Wiegandt (1982b) criterion for bifurcation can be deduced from the current theory, provided isotropic residual velocity distribution is assumed along the equatorial plane, also for triaxial configurations. On the other hand, the above assumption is in contradiction with Eqs. (59) and then it cannot be accepted. A criterion for bifurcation, consistent with Eqs. (59), is expressed by Eq. (119).

The origin of the discrepancy could be the following. Wiegandt (1982a) assumption (ii) implies Eq. (12) therein which, after integration, yields isotropic residual velocity distribution along the equatorial plane i.e.  $\zeta_{11} = \zeta_{22}$ . On the other hand, an isotropic residual velocity distribution along the equatorial plane is related to a zero-th order approximation in some special series developments [Marochnik 1967; Eq. (19) therein]. The additional requirement of axial symmetry makes the above mentioned relation be exact, but in presence of triplanar symmetry it has to be considered as a zero-th order approximation.

In the light of the results discussed in the current subsection, the analogy between the behaviour of collisional and collisionless self-gravitating fluids, subjected to the restrictions (Wiegandt 1982a,b): (i) rigid rotation; (ii) constant residual velocity on the boundary; (iii) absence of internal energy transports; appears to be complete.